Available online at www.sciencedirect.com
SCIENCE DIRECT®
ELSEVIER
Nuclear Physics A 716 (2003) 3–54
NUCLEAR PHYSICS A
www.elsevier.com/locate/npe

Nuclear structure of ^{129}Te studied with (n, γ), (d, p) and ($\vec{\text{d}}$, t) reactions

H.-F. Wirth [a,*,1], T. von Egidy [a], I. Tomandl [b], J. Honzátko [b], D. Bucurescu [c], N. Mărginean [c], V.Yu. Ponomarev [d], R. Hertenberger [e], Y. Eisermann [e], G. Graw [e]

[a] *Physik-Department, Technische Universität München, D-85748 Garching, Germany*
[b] *Nuclear Physics Institute, 250 68 Řež, Czech Republic*
[c] *Horia Hulubei Institute of Physics and Nuclear Engineering, 76900 Bucharest, Romania*
[d] *Joint Institute for Nuclear Research, 141980 Dubna, Russia*
[e] *Sektion Physik, Ludwig-Maximilians-Universität München, D-85748 Garching, Germany*

Received 1 October 2002; received in revised form 18 November 2002; accepted 28 November 2002

Abstract

The nuclear structure of ^{129}Te has been investigated with the ^{128}Te(n, $\gamma\gamma$)^{129}Te reaction using thermal neutrons, with the ^{128}Te(d, p)^{129}Te reaction at $E_{\text{d}} = 24$ MeV and $E_{\text{d}} = 18$ MeV, and with the ^{130}Te($\vec{\text{d}}$, t)^{129}Te reaction at $E_{\text{d}} = 24$ MeV. More than 110 levels were identified already below 3 MeV excitation energy, in most cases including spin, parity, and γ decay. The neutron binding energy was determined to be 6082.42(11) keV. The thermal neutron capture cross sections to the ground state and to the $11/2^-$ isomer were found to be 0.165(20) b and 0.021(3) b, respectively. The mechanism of direct neutron capture was verified to play an important role in the ^{128}Te(n, γ)^{129}Te reaction. The experimental level scheme is compared with predictions of the Interacting Boson–Fermion Model (IBFM) and of the Quasiparticle Phonon Model (QPM).

PACS: 21.10.-k; 21.10.Jx; 21.60.Ev; 27.60.+j

Keywords: NUCLEAR REACTIONS ^{128}Te(n, γ), E = thermal; Measured E_γ, I_γ, $\gamma\gamma$ coincidence; ^{128}Te(d, p), $E = 18, 24$ MeV; ^{130}Te(polarized d, t), $E = 24$ MeV; Measured particle spectra, angular distributions; ^{129}Te deduced levels, J, π, binding energy; Comparison with model predictions

* Corresponding author.
E-mail address: hans-friedrich.wirth@lmu.de (H.-F. Wirth).
[1] Present address: Sektion Physik, Ludwig-Maximilians-Universität München, Am Coulombwall 1, D-85748 Garching, Germany.

0375-9474/02/$ – see front matter
doi:10.1016/S0375-9474(02)01401-X

1. Introduction

The long chain of tellurium isotopes from ^{119}Te to ^{131}Te has been investigated by our collaboration via (n, γ) and/or one-nucleon transfer reactions: ^{119}Te [1], ^{121}Te [2], ^{122}Te [3], ^{123}Te [4], ^{124}Te [5,6], ^{125}Te [7], ^{126}Te [8], ^{127}Te [9,10], ^{129}Te [11,12] and ^{131}Te [13, 14]. These tellurium isotopes with two protons above the $Z = 50$ shell closure and $N = 67$ to $N = 79$ neutrons are interesting for many reasons. The low number of valence nucleons of one kind (protons) and the wide range of valence nucleons of the other kind (from the middle between the $N = 50$ and $N = 82$ shells to nearly $N = 82$) is especially suitable for testing and the development of nuclear models. Such nuclei cannot be described any more with the one-particle shell model or the Nilsson model which assumes a deformed ground state. Good results can be achieved with the interacting boson–fermion model (IBFM) or the quasiparticle phonon model (QPM) which describe the excited states in a collective way, i.e., they take into account a larger number of nucleons.

In this publication we report in detail on the nuclear structure investigations of ^{129}Te via (n, $\gamma\gamma$), (d, p) and ($\vec{\text{d}}$, t) reactions. The observation of non-statistical effects like direct neutron capture and the exceptionally strong isomer population make the second-heaviest tellurium isotope in the chain we studied particularly interesting.

The nucleus ^{129}Te was previously studied via the β^- decay of ^{129}Sb [15,16], the (n, γ) reaction [17], the (p, d) reaction [18], the (d, p) reaction [19], the (d, t) reaction [20], the (t, d) reaction [21], and the (^{3}He, α) reaction [18]. The results of these measurements are compiled in the Nuclear Data Sheets [22].

2. Experimental procedures and results

2.1. Thermal neutron capture studies

Thermal neutron capture studies on ^{128}Te were performed with two HPGe semiconductor detectors at the light-water reactor LWR-15 at Řež near Prague, where a special setup for the measurement of $\gamma\gamma$ coincidences is installed [23]. A 28% HPGe detector with a resolution of 2 keV at 1332 keV (^{60}Co line) and about 5 keV at 6 MeV and a 22% detector with approximately the same resolution were applied. For both detectors a new relative efficiency calibration was made with the radioactive sources ^{152}Eu, ^{133}Ba and ^{60}Co, and with the reaction ^{35}Cl(n, γ). The energies and intensities of these lines were taken from the Refs. [24,25]. The absolute intensity calibration of the ^{129}Te spectra was made with the 459.6 keV line of ^{129}I from the activation of ^{129}Te and independently with a sandwich target of tellurium and aluminum, where the 1779.0 keV line of ^{28}Si from the β-decay of ^{28}Al was used. The target consisted of 1.8 g metallic Te enriched in ^{128}Te to 99.3%. Two single spectra were measured with both detectors simultaneously, one in the energy range from 0 MeV to 1.6 MeV, and the other one from 0 MeV up to 6 MeV. The energy calibration was made using prominent background lines and with the help of a ^{128}Te(n, γ) measurement of Stone et al. [26]. Background from other Te isotopes, especially ^{124}Te in the target, was identified using the Refs. [5,27,28].

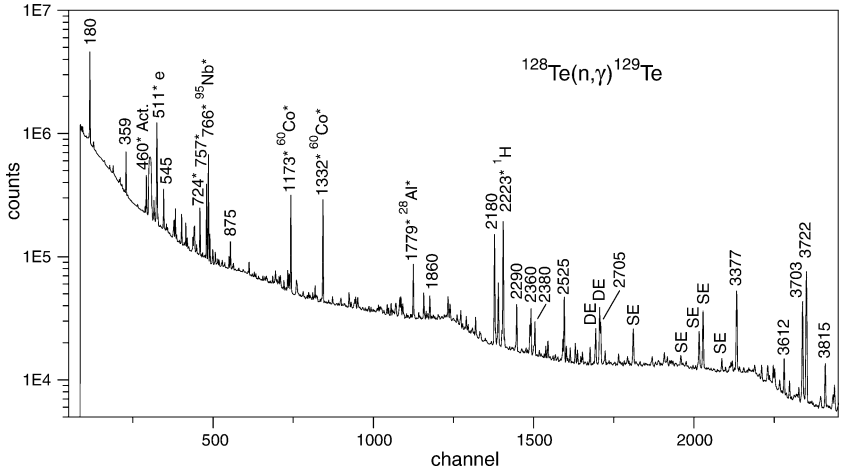

Fig. 1. Part of a ^{128}Te(n, γ)^{129}Te spectrum. Some lines are labeled with their energy in keV. Lines not belonging to ^{129}Te are marked with an asterisk. The asterisk after the given isotopes means that the γ line stems from radioactive decay and the lines are transitions in the daughter nuclei. SE and DE stand for single and double escape after pair production, respectively.

A part of one single spectrum is shown in Fig. 1. Besides many lines of ^{129}Te which are labeled with their energy in keV, some background lines are marked with an asterisk. To identify clearly γ lines from the reaction ^{128}Te(n, γ)^{129}Te a background measurement with only a carbon target was performed. In this way we obtained a spectrum of the spurious lines in the γ spectra of ^{129}Te. Many background lines could be assigned using Ref. [29] and the online service of the NNDC.

For the generation of the coincidence spectra the energy signals of both detectors and their time difference were recorded as raw data. From these raw data one could later derive spectra of one detector in coincidence with a line (the gate) in the other detector. The second possibility was to set a gate on the sum of both detector signals and to look at the spectrum of one detector. The coincidence data were recorded with the 1.8 g ^{128}Te target in a run of about 400 hours at a reactor power of 9 MW and at a coincident counting rate of approximately 100 Hz. From these data we could get more than hundred meaningful coincidence spectra and eight productive so-called TSC (two step cascade) spectra.

Fig. 2 shows parts of the two most powerful coincidence spectra, those of the lines at 180 keV and 359 keV. The line 180 keV is the strongest line feeding the ground state of ^{129}Te and 359 keV the strongest line which feeds the isomer at 106 keV. This means that all lines in the spectra should be placed above the lines on which was gated. Now one can look at the coincidence spectra of these lines and construct step by step the whole level and decay scheme. On the other hand, several conditions have to be fulfilled before a new level is introduced, as will be precised later.

Another possibility, as mentioned above, is the generation of so-called TSC spectra. These spectra contain only pairs of coincident lines whose sum equals the energy on which is gated.

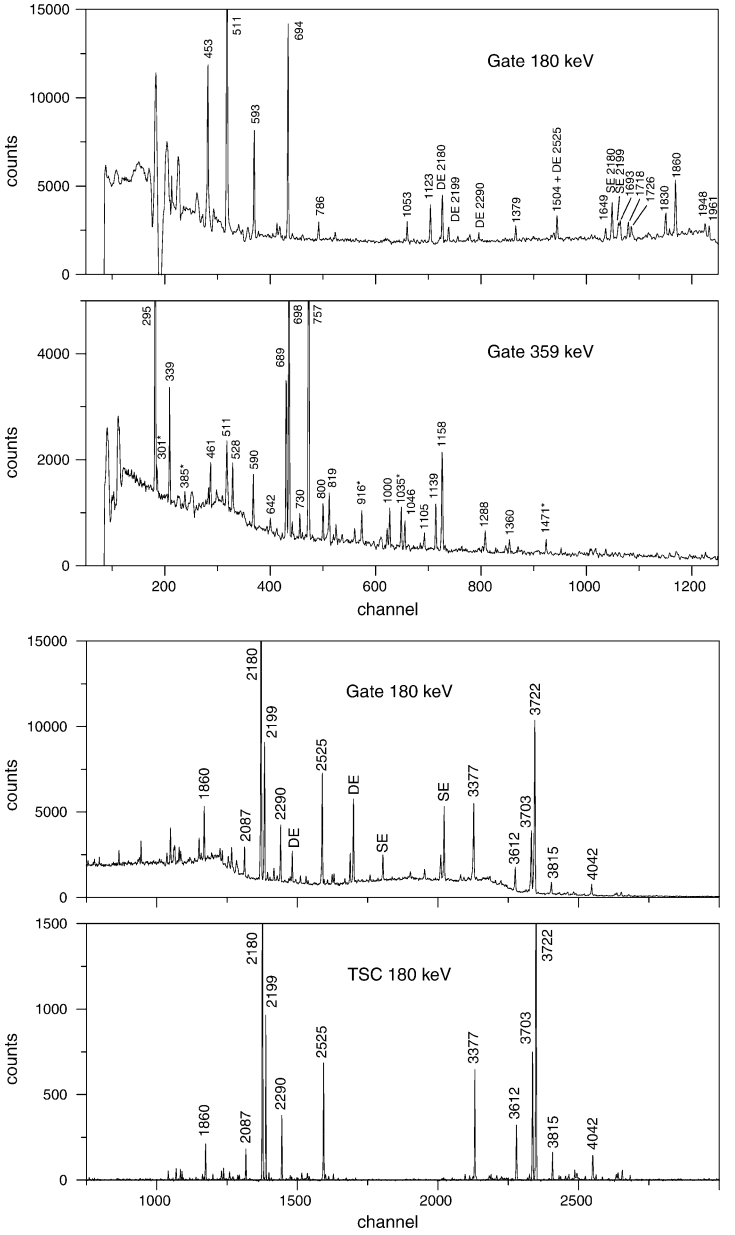

Fig. 2. Upper spectra: $\gamma\gamma$-coincidence spectra of the gates 180 keV and 359 keV. Some lines are labeled with their energy in keV. Lines that were later not placed in the level scheme of ^{129}Te are marked with an asterisk. The noticeable structure below channel 200 in the upper spectrum is artificial. Lower spectra: Parts of (n, $\gamma\gamma$) spectra with γ lines feeding the first excited state of ^{129}Te at 180 keV. The 'Gate 180 keV' spectrum is gated on the 180 keV line. The lower one is a two step cascade spectrum with γ lines from the capturing state at 6082 keV to the 180 keV level; the gate is the energy sum of 5902 keV (= (6082 − 180) keV) of two coincident lines. Numbers: energies in keV.

Fig. 2 shows in the lower part another section of the 180 keV coincidence spectrum which is shown on top of Fig. 2. This one is compared to the 180 keV TSC spectrum. In the TSC spectrum the gate was 5902 keV, which is the energy difference between the capturing state (6082 keV) minus the energy 180 keV. One observes pairs of γ lines which lie mirror-symmetrically around an apparent axis at 2952 keV and whose energy sum is 5902 keV. It follows that one γ line of a pair feeds the state at 180 keV directly, while the other one is a primary γ transition. This means that at 180 keV + E_γ there has to be a level of ^{129}Te, but one does not know the order of the γ lines. This ambiguity has to be removed with the help of other coincidence spectra or the transfer measurements. Besides their importance for the construction of the level scheme the TSC spectra are also very helpful for identifying background. While in the normal coincidence spectra there are no lines from other isotopes (if the gate does not contain background) in the TSC spectra there are also no single or double escape lines.

Table 1 contains all γ lines considered to belong to ^{129}Te with energy and absolute intensity. Their placement in the level scheme is also given, even if this anticipates Section 3. To get background-free intensities its contribution was subtracted for some lines with the help of coincidence spectra or with the help of the background measurement. The obtained intensities are in very good agreement with values of an earlier measurement of Honzátko et al. [17].

Table 1
Gamma transitions following thermal neutron capture in ^{128}Te. If the line is not placed, coincident lines (E_γ in keV) are given. The systematic error of the listed intensities is about 10% and has to be added to the given statistical error. The γ energies E_γ are not corrected for recoil

E_γ (keV)	I_γ (γs/100 n)	$(\Delta I/I)$ (%)	E_i (keV)	→	E_f (keV)
149.65(5)	0.31	4		453	
180.33(3)	44.03	1	180	→	0
188.42(23)	0.05	17		—	
230.1(3)	0.04	25		—	
295.27(4)	1.23	2	760	→	465
300.81(14)	0.10	12		359, 698, 916	
330.32(5)	1.10	2	875	→	545
338.65(8)	0.45	6	1560	→	1221
344.55(10)	0.22	6	2705	→	2360
359.19(5)	7.60	1	465	→	106
364.26(10)	0.15	9	545	→	180
367.90(7)	0.23	16		1649	
380.2(3)	0.07	15		—	
384.75(17)	0.11	9		359, 1035	
391.6(4)	0.05	22		—	
416.67(9)	0.27	15		819	
427.7(3)	0.05	17	4221	→	3792
437.4(4)	0.07	18	2705	→	2267
439.9(4)	0.07	17		—	
443.5(4)	0.06	22		—	
453.33(3)	1.01	2	634	→	180
461.47(5)	0.65	5	1221	→	760
480.22(21)[a]	0.28	15	2040	→	1560

Table 1 (*continued*)

E_γ (keV)	I_γ (γs/100 n)	$(\Delta I/I)$ (%)	E_i (keV)	→	E_f (keV)
527.90(8)	0.22	5	2380	→	1851
531.46(20)	0.08	14		—	
544.61(3)	5.37	1	545	→	0
546.98(16)	0.11	10		—	
590.00(9)	0.20	6	1753	→	1162
592.81(3)	0.89	2	773	→	180
599.34(23)	0.10	14		—	
623.87(20)	0.09	13	2493	→	1869
633.78(3)	3.92	1	634	→	0
637.61(21)	0.08	14		2652	
641.84(17)	0.11	11	2493	→	1851
648.11(10)	0.19	6	1421	→	773
654.30(3)	2.85	1	760	→	106
666.98(14)	0.18	8		545	
669.64(8)	0.25	5	1303	→	634
684.6(3)	0.17	7	1318	→	634
689.22(9)[b]	0.40	15	1234	→	544
689.22(9)[b]	1.01	9	1851	→	1162
694.49(3)	2.17	1	875	→	180
697.59(3)	2.67	1	1162	→	465
704.40(18)	0.14	9	2360	→	1656
707.21(15)	0.41	14	2267	→	1560
723.22(14)[a]	0.11	15	2380	→	1656
729.97(10)	0.19	7	2582	→	1851
736.94(6)	0.38	4	1281	→	545
756.59(3)[c]	3.08	11	1221	→	465
773.22(3)[b]	2.79	7	773	→	0
773.22(3)[b]	0.10	20	1318	→	545
786.45(7)[d,e]	0.42	7	967	→	180
786.45(7)[d]	0.42	7	1560	→	773
786.45(7)[d]	0.42	7	1599	→	813
800.04(3)	0.63	11	1560	→	760
800.40(20)[a]	0.48	15	2360	→	1560
812.93(7)	0.54	3	813	→	0
818.86(6)	0.43	3	2040	→	1221
857.1(6)	0.04	31		359	
874.78(4)	3.18	1	875	→	0
885.0(3)	0.11	13	1851	→	967
889.0(3)	0.09	15		—	
916.13(12)	0.22	6		359	
874.78(4)	3.18	1		301, 359, 698	
937.4(3)	0.10	14		—	
945.7(4)	0.07	18		—	
966.87(7)	1.25	2	967	→	0
981.6(5)	0.08	17		—	
984.1(4)	0.10	15		—	
992.52(8)	0.43	4	1753	→	760
996.3(4)	0.09	17		—	
1000.26(10)	0.34	4	2222	→	1221
1034.97(9)	0.36	4		295, 359, 385, 698	

Table 1 (*continued*)

E_γ (keV)	I_γ (γs/100 n)	$(\Delta I/I)$ (%)	E_i (keV)	→	E_f (keV)
1045.83(10)	0.36	5	2267	→	1221
1053.36(19)	0.36	6	1234	→	180
1056.53(16)	0.21	7	1162	→	106
1072.34(23)	0.14	10		359	
1091.42(23)	0.14	11	1851	→	760
1095.47(18)	0.26	8	1869	→	773
1097.9(3)[a]	0.49	9	2380	→	1281
1105.46(11)	0.20	10	2267	→	1162
1123.01(7)	0.57	4	1303	→	180
1126.10(24)	0.10	17		—	
1139.21(13)	0.39	8	2360	→	1221
1150.17(23)	0.13	13		—	
1155.57(15)	0.23	8		—	
1158.37(12)	0.83	5	2380	→	1221
1208.3(3)	0.12	13		—	
1211.9(3)	0.13	12		—	
1221.23(13)	0.13	12	1221	→	0
1232.4(3)	0.21	10		—	
1234.5(3)	0.26	8	1869	→	634
1253.87(21)	0.18	10		634	
1273.5(3)	0.11	13		—	
1281.59(10)	0.39	7	1281	→	0
1287.62(18)	0.20	9	1753	→	465
1301.5(4)	0.18	12		—	
1303.6(4)	0.23	10	1303	→	0
1318.54(22)	0.16	10	1318	→	0
1324.6(3)	0.21	9	1869	→	545
1338.8(3)	0.15	16		—	
1342.2(5)	0.10	23		773	
1358.1(7)	0.10	23		—	
1360.4(4)	0.17	15	2582	→	1221
1379.33(19)	0.18	18	1560	→	180
1401.4(3)	0.13	13	2705	→	1303
1412.4(5)	0.08	25	2380	→	967
1418.07(21)	0.33	7		—	
1421.36(15)	0.48	5	1421	→	0
1439.7(4)	0.15	14		—	
1470.9(4)[f]	0.27	16	2705	→	1234
1485.48(16)	0.33	6	2360	→	875
1493.91(12)[b]	0.29	15	2267	→	773
1493.91(12)[b]	0.45	10	6082	→	4589
1504.3(3)	0.57	16	2380	→	875
1514.2(4)	0.16	12		359	
1526.4(6)	0.11	25	2493	→	967
1529.55(22)	0.15	18		—	
1541.1(3)	0.16	15		—	
1549.0(5)	0.10	23		—	
1556.53(5)	0.11	17		—	
1559.66(21)	0.39	5	1560	→	0
1569.84(23)	0.28	16		757	

Table 1 (*continued*)

E_γ (keV)	I_γ (γs/100 n)	$(\Delta I/I)$ (%)	E_i (keV)	→	E_f (keV)
1586.7(5)	0.14	31	2360	→	773
1606.60(13)	0.60	8	2380	→	773
1617.95(16)	0.52	10		—	
1619.5(6)[a]	0.34	12	2380	→	760
1633.6(3)	0.26	18	2267	→	634
1649.47(9)[b]	0.48	20	6082	→	4433
1649.47(9)[b]	0.31	30	2525	→	875
1656.29(13)	0.52	10	1656	→	0
1677.29(15)	0.48	11	2222	→	545
1682.50(23)	0.31	15		—	
1693.45(10)	0.93	7	6082	→	4389
1708.4(3)[d]	0.50	13	4087	→	2380
1708.4(3)[d]	0.50	13	6082	→	4374
1717.80(5)	1.76	3	6082	→	4365
1726.24(7)	0.28	19	6082	→	4356
1731.9(3)	0.27	18		—	
1745.7(3)	0.24	20	2380	→	634
1752.6(4)	0.17	29	1753	→	0
1770.41(20)	0.25	8		—	
1784.58(23)	0.22	17	6082	→	4298
1805.35(11)	0.40	5	6082	→	4277
1815.6(5)	0.08	23	2360	→	545
1830.22(4)	2.12	1	2705	→	875
1834.9(3)	0.26	8	2380	→	545
1842.1(3)	0.49	4	6082	→	4240
1848.3(5)	0.14	17		—	
1851.28(18)	0.37	7	1851	→	0
1859.64(8)	1.51	3	2040	→	180
1861.80(18)	0.58	8	6082	→	4221
1878.1(3)	0.28	17	6082	→	4204
1901.77(18)	0.34	11	6082	→	4181
1906.9(3)	0.20	18	6082	→	4175
1920.7(3)	0.21	18		2290	
1931.91(23)	0.31	15	2705	→	773
1948.81(10)[a]	0.61	21	6082	→	4133
1961.16(8)[a]	0.63	31	6082	→	4121
1987.6(6)[a]	0.05	24	3547	→	1560
1994.92(12)	0.68	8	6082	→	4087
1999.5(3)	0.24	21	4221	→	2222
2022.67(20)[g]	0.34	8		—	
2040.38(7)	0.71	6	2040	→	0
2041.6(7)[a]	0.34	4	2222	→	180
2049.87(16)	0.51	6	6082	→	4033
2059.6(4)	0.17	16		—	
2066.7(3)	0.30	9		—	
2071.03(23)	0.43	7	2705	→	634
2079.5(3)	0.24	11		—	
2086.84(6)	1.32	2	2267	→	180
2107.30(15)[g]	0.44	8		—	
2134.5(3)	0.18	14		—	

Table 1 (*continued*)

E_γ (keV)	I_γ (γs/100 n)	$(\Delta I/I)$ (%)	E_i (keV)	→	E_f (keV)
2164.9(4)	0.14	18		—	
2180.12(3)	17.22	3	2360	→	180
2194.03(14)	0.46	7		—	
2199.21(3)	5.70	1	2380	→	180
2216.96(7)	0.85	4	6082	→	3865
2221.5(4)[a]	0.98	14	2222	→	0
2229.63(13)	0.53	4	6082	→	3853
2267.1(9)	0.12	26	2267	→	0
2289.99(4)	3.83	1	6082	→	3792
2312.7(8)	0.12	25	2493	→	180
2336.4(3)	0.25	8		—	
2343.7(3)	0.19	9	2525	→	180
2360.42(3)	3.22	1	2360	→	0
2371.1(7)	0.11	18	3792	→	1421
2374.71(20)	0.46	5		—	
2379.51(4)	2.06	2	2380	→	0
2401.74(22)	0.27	7	2582	→	180
2410.0(5)	0.12	14		654, 773	
2433.65(11)	0.56	5	6082	→	3649
2443.99(7)	0.97	3	6082	→	3638
2480.44(24)	0.25	9		—	
2493.1(6)	0.14	20	2493	→	0
2518.02(11)	1.14	2	6082	→	3564
2524.78(3)[b]	4.78	7	2705	→	180
2524.78(3)[b]	1.08	30	2525	→	0
2535.47(9)	0.79	4	6082	→	3547
2542.7(4)	0.16	15		—	
2554.06(10)	0.43	18	6082	→	3528
2554.0(5)[a]	0.26	30	3430	→	875
2579.78(7)	1.06	3	6082	→	3502
2581.5(9)[a]	0.09	26	2582	→	0
2606.89(20)	0.33	7		—	
2627.7(5)	0.12	18	3502	→	875
2630.0(11)	0.08	34	3853	→	1221
2652.3(4)[b]	0.19	30	3528	→	875
2652.3(4)[b]	0.65	9	6082	→	3430
2670.4(6)	0.11	21	3430	→	760
2705.07(4)	3.23	1	2705	→	0
2721.6(5)	0.16	15		—	
2726.70(12)	0.68	4	6082	→	3356
2741.4(11)	0.07	34	3502	→	760
2754.8(7)	0.14	19	3528	→	773
2837.35(20)	0.53	5		—	
2878.8(6)	0.21	13		—	
2898.9(4)	0.22	12		—	
2989.3(5)	0.31	11		—	
2994.0(6)	0.23	15		—	
3018.7(10)[a]	0.11	26	3792	→	773
3046.5(3)	0.29	12		—	
3053.7(3)	0.31	11		—	

Table 1 (*continued*)

E_γ (keV)	I_γ (γs/100 n)	$(\Delta I/I)$ (%)	E_i (keV)	→	E_f (keV)
3127.1(3)	0.34	10		—	
3237.3(9)	0.11	21		—	
3250.0(10)	0.10	22	3430	→	180
3322.0(4)	0.28	9	3502	→	180
3348.6(5)	0.64	5	3528	→	180
3355.14(14)	0.73	5	3356	→	0
3366.3(6)	0.22	15	3547	→	180
3377.26(4)	10.44	1	6082	→	2705
3391.2(3)	0.27	12		—	
3412.2(4)	0.27	12		—	
3457.6(3)	0.33	10	3638	→	180
3468.7(3)	0.39	13	3649	→	180
3500.59(12)	0.86	5	6082	→	2582
3528.4(4)	0.54	15	3528	→	0
3545.1(5)	0.17	18		—	
3546.6(11)[a]	0.05	24	3547	→	0
3557.60(9)	1.16	3	6082	→	2525
3564.71(14)	1.04	4	3564	→	0
3589.41(17)	0.52	6	6082	→	2493
3601.1(10)	0.08	34		—	
3612.02(6)	2.14	2	3792	→	180
3638.36(13)	0.69	5	3638	→	0
3672.2(3)	0.26	12	3853	→	180
3684.74(14)	0.55	6	3865	→	180
3702.82(6)	10.33	1	6082	→	2380
3721.87(5)	19.54	1	6082	→	2360
3787.7(7)	0.14	15		—	
3792.4(3)	0.39	6	3792	→	0
3815.14(6)	2.39	2	6082	→	2267
3824.1(7)	0.12	16		—	
3849.8(6)	0.24	13		—	
3853.6(7)	0.50	6	4033	→	180
3860.59(10)	1.00	3	6082	→	2222
3876.7(7)	0.13	16		—	
3882.2(4)[h]	0.30	7		—	
3888.7(6)	0.14	14		—	
3902.14(12)[i]	0.85	3		—	
3907.2(5)	0.25	9	4087	→	180
3940.4(4)	0.24	9	4121	→	180
3952.8(4)	0.26	8	4133	→	180
4001.5(8)	0.22	10	4181	→	180
4042.11(7)	2.09	2	6082	→	2040
4060.5(5)	0.21	10	4240	→	180
4076.7(6)	0.15	14		—	
4096.5(3)[a]	0.10	26	4277	→	180
4120.5(4)[a]	0.06	21	4121	→	0
4133.23(19)	0.46	5	4133	→	0
4174.6(6)	0.32	9	4175	→	0
4174.6(6)	0.32	9	4356	→	180
4184.0(3)	0.44	6	4365	→	180

Table 1 (*continued*)

E_γ (keV)	I_γ (γ_s/100 n)	$(\Delta I/I)$ (%)	E_i (keV)	→	E_f (keV)
4204.0(9)	0.21	19	4204	→	0
4208.4(4)	0.44	9	4389	→	180
4246.0(8)	0.24	12		—	
4252.0(6)	0.23	10	4433	→	180
4297.7(6)	0.17	13	4298	→	0
4364.38(15)	0.83	3	4365	→	0
4374.6(12)	0.07	31	4374	→	0
4390.1(4)	0.24	9		—	
4407.0(5)	0.22	10		—	
4426.8(7)	0.23	11	6082	→	1656
4433.6(5)	0.65	4	4433	→	0
4523.0(5)	0.23	9	6082	→	1560
4588.5(5)	0.21	12	4589	→	0
4859.8(11)	0.08	22		—	
4903.4(8)	0.21	13		—	
4919.6(10)	0.11	17		—	
5049.7(9)	0.12	17		—	
5133.8(8)	0.17	13		—	
5449.4(6)	0.22	11	6082	→	634
5901.55(24)	0.59	5	6082	→	180
6082.0(3)	0.39	6	6082	→	0

[a] Energy and intensity of the line from coincidence spectra.
[b] Multiply placed. Intensity division with the help of coincidence spectra.
[c] Intensity from coincidence spectra.
[d] Multiply placed. Undivided intensity given.
[e] Placement not confirmed by coincidences.
[f] Placement not unique, because also observed in coincidence with 359 keV.
[g] Probably primary transition.
[h] Probably enhanced by angular correlation (180 keV + 3702 keV).
[i] Probably enhanced by angular correlation (180 keV + 3722 keV).

2.2. *The* (d, p) *measurement at* $E_d = 24$ MeV

The ^{128}Te(d, p)^{129}Te measurement at $E_d = 24$ MeV was carried out with an unpolarized deuteron beam at the Tandem Accelerator Laboratory of the University and the Technical University of Munich. The target consisted of 165 μg/cm^2 metallic ^{128}Te (enrichment 99.3%) evaporated on a 4 μg/cm^2 thick carbon foil. The reaction products were analyzed with the Q3D magnetic spectrograph [30] and detected in its 1.8 m long focal plane. The detector was a multiwire proportional counter with $\Delta E/E_{rest}$ particle identification for background suppression [31]. The integration of the beam current in a Faraday cup after passing the target allowed the calculation of absolute cross sections. We measured at 12 scattering angles between 10° and 40°. Fig. 3 shows in the upper part a spectrum at $\theta_{lab} = 25°$. The measuring time was 1.5 h at a beam current of 300 nA on target and an acceptance solid angle of the Q3D spectrograph of 1.4 msr. The achieved energy resolution was about 5 keV (FWHM). Up to an excitation energy of 2980 keV we evaluated 64 angular distributions. The energy calibration was done via the aid of known levels from the NDS [22] and the (n, $\gamma\gamma$) measurement starting at low excitations. Assuming a polynomial

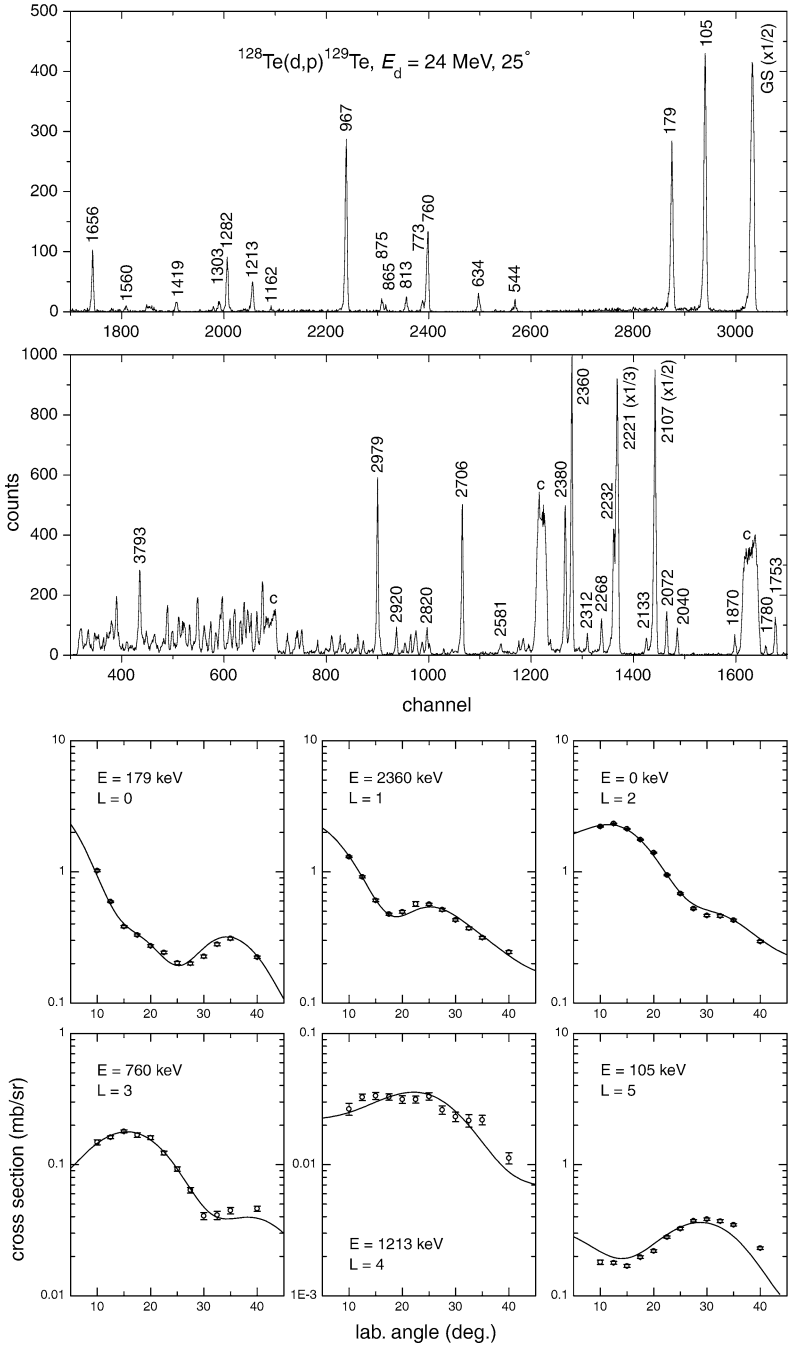

Fig. 3. Upper part: Spectrum of the ^{128}Te(d, p)^{129}Te reaction at $E_d = 24$ MeV and $\theta_{lab} = 25°$. Some levels are labeled with their energy in keV. c: background of light elements in the target. Lower part: Typical angular distributions of the cross section for $l = 0$ to $l = 5$. The solid lines are the results of DWBA calculations.

of 2nd order (relation between detector channel and excitation energy) for the energy calibration one can recognize and add levels of higher excitation step by step. Due to the ion optical properties of the Q3D a 3rd order polynomial for the energy calibration was finally needed. The fitting procedure was done with the program GASPAN of F. Rieß [32].

Some typical angular distributions of the cross section are given in the lower part of Fig. 3. They are very well reproduced by DWBA (distorted wave Born approximation) calculations. The potential parameters for these calculations will be given in Section 2.6.

2.3. The (d, p) *measurement at* $E_d = 18$ MeV

To reach better statistics at higher excitation energies the reaction ^{128}Te(d, p)^{129}Te was measured again at another magnetic setting of the Q3D spectrograph. In this experiment the deuteron energy was reduced to $E_d = 18$ MeV. The target consisted of 145 µg/cm^2 metallic ^{128}Te (enrichment 99.3%) evaporated on a 4 µg/cm^2 thick carbon foil. We measured at 11 scattering angles between 10° and 50°. Fig. 4 shows one spectrum at $\theta_{lab} = 25°$. The measuring time was 1.5 h at a beam current of 250 nA on the target and an acceptance solid angle of the Q3D spectrograph of 4.4 msr. The achieved energy resolution was excellent 4 keV (FWHM) in the best region (the middle) of the detector. Between 2040 keV and 5013 keV excitation energy we evaluated 232 angular distributions. The aim

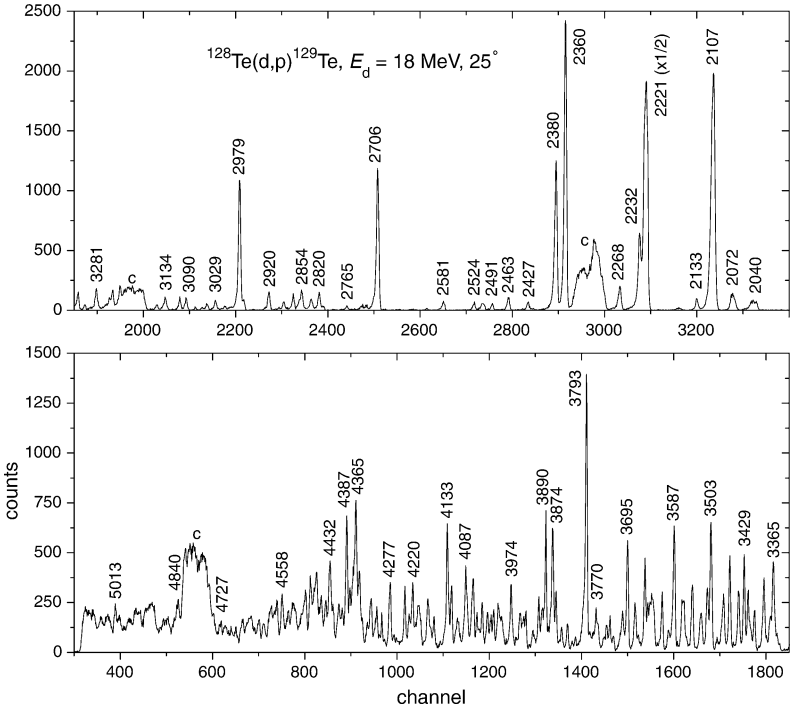

Fig. 4. Spectrum of the ^{128}Te(d, p)^{129}Te reaction at $E_d = 18$ MeV and $\theta_{lab} = 25°$. Some levels are labeled with their energy in keV. c: background of light elements in the target.

of this measurement was to identify the $l = 1$ transfers that are of special interest for the mechanism of the so-called direct capture, as will be seen later. Because of the changed beam energy the shape of the angular distributions differs slightly from that shown in Fig. 3, but the $l = 1$ transfers remain easy to recognize.

2.4. The $(\vec{\mathrm{d}}, \mathrm{p})$ measurement at $E_\mathrm{d} = 18$ MeV

Especially to distinguish between $1/2^-$ and $3/2^-$ states we measured the neutron stripping reaction again, but this time with polarized deuterons. The $^{128}\mathrm{Te}(\vec{\mathrm{d}}, \mathrm{p})^{129}\mathrm{Te}$ measurement was carried out at one scattering angle of $\theta_\mathrm{lab} = 22°$, where DWBA calculations predicted the strongest analyzing power for the $l = 1$ transfer. The experimental analyzing power was deduced from the equation

$$A_y = \frac{2}{3P_3}\frac{\sigma_+ - \sigma_-}{\sigma_+ + \sigma_-}, \tag{1}$$

where σ_+ and σ_- are the measured differential cross sections with respect to the polarization of the beam and where P_3 is the vector polarization. The value of the vector polarization P_3 of the beam coming from a new atomic beam source was about 70% [33]. The target was the same as in the unpolarized measurement (see above). The focal plane detector was this time a new cathode strip detector with single strip readout [12, 34], which is able to handle higher beam currents (> 1 μA). Fig. 5 shows two spectra

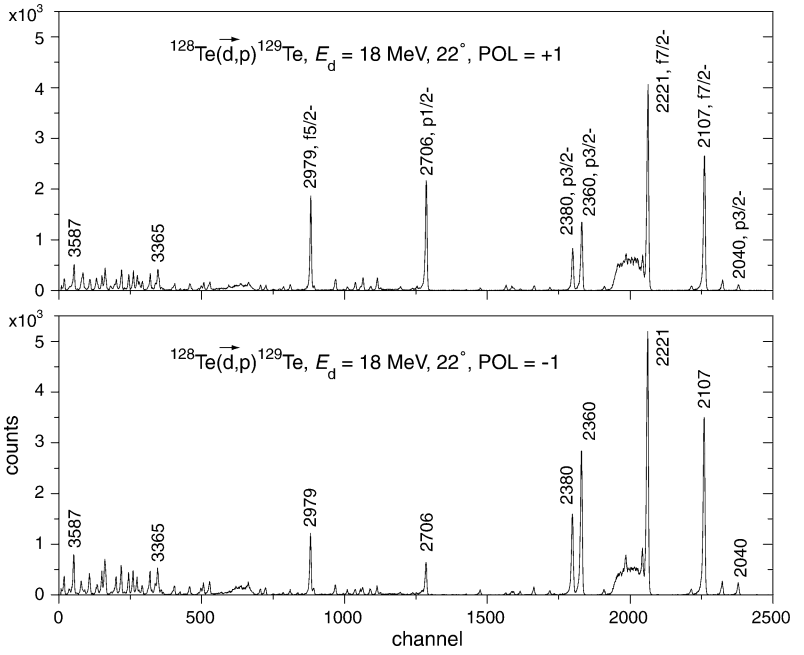

Fig. 5. Spectra of the $^{128}\mathrm{Te}(\vec{\mathrm{d}}, \mathrm{p})^{129}\mathrm{Te}$ reaction at $\theta_\mathrm{lab} = 22°$. Some levels are labeled with their excitation energy in keV and with their spin and parity assignment. The POL $= -1$ spectrum is scaled to the same charge on the target as the POL $= +1$ spectrum.

out of four that were measured. (The two others were measured at another magnetic setting of the spectrograph to reach higher excitation energies.) The energy resolution was excellent 4 keV over the whole spectrum. The effect of the polarization is clearly visible in Fig. 5, especially for the $1/2^-$ and $3/2^-$ states. In this way many spin assignments of the $l = 1$ states identified in our earlier measurement of the angular distributions of ^{128}Te(d, p)^{129}Te became unambiguous. The analyzing power was also used to derive unambiguous assignments for some $l = 3$ levels like the $5/2^-$ state at 2979 keV and the $7/2^-$ state at 2107 keV.

2.5. *The* $(\vec{\mathrm{d}}, \mathrm{t})$ *measurement at* $E_\mathrm{d} = 24$ MeV

Angular distributions of the reaction ^{130}Te$(\vec{\mathrm{d}}, \mathrm{t})^{129}$Te have been measured at a deuteron energy of $E_\mathrm{d} = 24$ MeV. The target consisted of 100 μg/cm^2 metallic ^{130}Te (enrichment 99.5%) evaporated on a 4 μg/cm^2 thick carbon foil. Fig. 6 shows the POL $= +1$ spectrum at $\theta_\mathrm{lab} = 20°$, recorded with the long multiwire proportional counter [31]. The measuring time was 1 h at 140 nA $\vec{\mathrm{d}}$ on the target and an acceptance solid angle of 11 msr. For ten angles in the range from 7.5° to 40° both spin directions have been measured. The achieved resolution was about 5–6 keV in the best region of the focal plane detector.

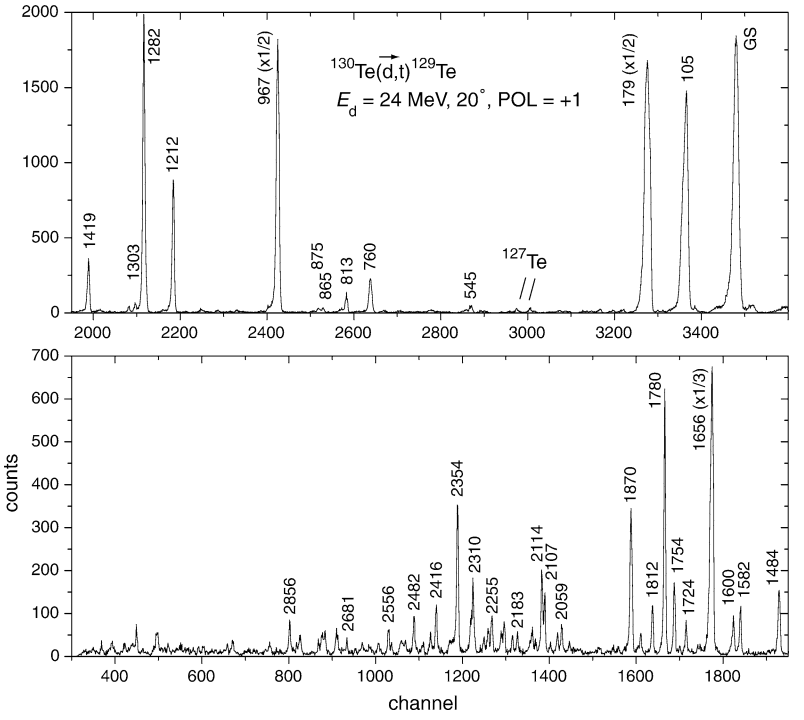

Fig. 6. Spectrum of the ^{130}Te$(\vec{\mathrm{d}}, \mathrm{t})^{129}$Te reaction at $E_\mathrm{d} = 24$ MeV, POL $= +1$ and $\theta_\mathrm{lab} = 20°$. Some levels are labeled with their excitation energy in keV. The two peaks marked with "^{127}Te" belong to the reaction ^{128}Te(d, t) ^{127}Te.

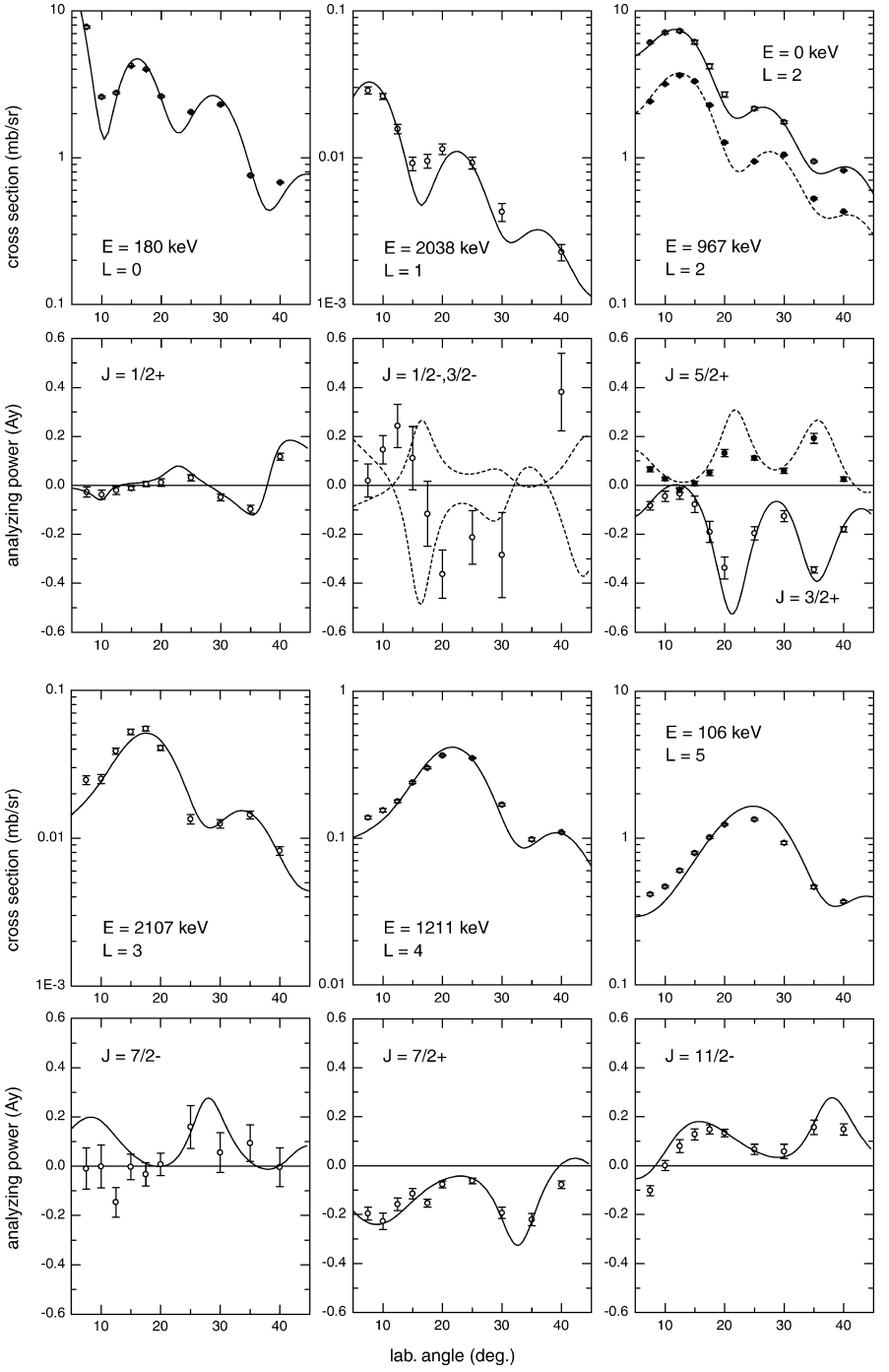

Fig. 7. Typical angular distributions of the ^{130}Te($\vec{\mathrm{d}}$, t)^{129}Te measurement at $E_{\mathrm{d}} = 24$ MeV.

The energy calibration was done following the same procedure as described in Section 2.2. Nevertheless, above 2100 keV the (d, t) levels cannot be easily compared with the levels populated by other reactions. Also a comparison with former pickup reactions is difficult as will be shown in Section 3. Therefore, the energy calibration had to be continued using a calibration measurement with a ^{208}Pb target. This caused an increasing systematic energy error of 5 keV at 3 MeV. The fact that the (d, t) reaction populates already above 1.5 MeV excitation energy other levels than the (d, p) and (n, γ) reactions can be understood as a clear hint for the different selectivity of the two latter reactions. This selectivity manifests itself in the unusual isomer population and the favoured direct neutron capture, as will be seen later.

Up to an excitation energy of 2860 keV 71 angular distributions of the absolute cross section and the analyzing power have been gained from the $(\vec{\mathrm{d}}, \mathrm{t})^{129}$Te measurement. The very good quality of the data can be seen in Fig. 7.

2.6. DWBA analysis

To deduce the angular momentum transfer and the spin of each state from the angular distributions DWBA calculations have been performed with the computer program CHUCK3 of P.D. Kunz [35]. Many systematic studies exist concerning the optical potential parameters needed for the input file ([36,37] and references therein). The parameters used in this work have been chosen to reproduce best the angular distributions, but we took care that their values stay within the known limits. Table 2 gives a summary of the parameters used for the three measured transfer reactions.

For the excited states in the (d, p) and (d, t) reactions shell model configurations of Table 3 for the neutron have been assumed. The number of nodes, defined as $n-1$ (n: main quantum number) is important for the DWBA calculations because it influences the spectroscopic factors. Fig. 17 in the Appendix shows three example input files for different states in the three measured transfer reactions. The CHUCK3 output files contain angular distributions for cross section and analyzing power. The ratio between measured and calculated cross sections is the spectroscopic factor S_{lj} in (d, p) and the spectroscopic strength G_{lj} in (d, t). This means:

$$\frac{d\sigma^{\exp}}{d\Omega} = S_{lj}\sigma_{lj}^{\mathrm{CHUCK3}} \quad \text{in (d, p)} \quad \text{and} \quad \frac{d\sigma^{\exp}}{d\Omega} = G_{lj}\sigma_{lj}^{\mathrm{CHUCK3}} \quad \text{in (d, t)},$$
$$\text{with } G_{lj} = (2j+1)S_{lj}.$$

The spectroscopic factor or strength has been determined for each level by fitting the calculated angular distributions through a factor to the measured ones.

The shape of the angular distribution of the cross section is very similar for the same l, but different J values $(l+1/2, l-1/2)$. The analyzing power observed in polarized measurements is needed to remove the ambiguity (cp. the upper part of Fig. 7), because it is clearly different for $J = l+1/2$ and $J = l-1/2$. It is not possible to derive unambiguous J assignments from an unpolarized measurement.

Figures of all measured and calculated angular distributions of the transfer reactions can be found in the appendix of Ref. [12].

Table 2
Optical potential parameters used in the DWBA calculations. FNRG = 0.621 for (d, p) and 0.845 for (d, t)

		^{128}Te(d, p), $E_d = 24$ MeV			^{128}Te(d, p), $E_d = 18$ MeV			^{130}Te(d, t), $E_d = 24$ MeV		
		d	p	n	d	p	n	d	t	n
V_r	(MeV)	105.93	51.96	[a]	113.17	56.12	[a]	96.50	150.24	[a]
$4W_D$	(MeV)	62.71	36.67		68.80	56.46		48.00		
W_0	(MeV)								20.00	
V_{so}	(MeV)	7.80	7.50	$\lambda = 25$	7.80	7.50	$\lambda = 25$	6.83		$\lambda = 25$
r_r	(fm)	1.12	1.22	1.17	1.12	1.22	1.17	1.13	1.24	1.17
r_D	(fm)	1.32	1.23		1.32	1.23		1.32		
r_0	(fm)								1.43	
r_{so}	(fm)	1.16	1.22		1.16	1.22		1.07		
R_c	(fm)	1.15	1.25		1.15	1.25		1.15	1.30	
a_r	(fm)	0.77	0.67	0.75	0.81	0.77	0.75	0.77	0.69	0.75
a_D	(fm)	0.85	0.67		0.91	0.77		0.68		
a_0	(fm)								0.87	
a_{so}	(fm)	0.84	0.67		0.84	0.67		0.66		
nlc		0.54	0.85	0.85	0.54	0.85	0.85	0.54	0.25	0.85

[a] Adjusted by CHUCK3.

Table 3
Adopted shell model configurations (neutron) of the levels in ^{129}Te

Reaction	Configuration	Number of nodes	Parity
(d, p)	$3p_{1/2}$	2	−
	$3p_{3/2}$	2	
	$2f_{5/2}$	1	
	$2f_{7/2}$	1	
	$1h_{11/2}$	0	
(d, p), (d, t)	$3s_{1/2}$	2	+
	$2d_{3/2}$	1	
	$2d_{5/2}$	1	
	$1g_{7/2}$	0	
	$1g_{9/2}$	0	
(d, t)	$2p_{1/2}$	1	−
	$2p_{3/2}$	1	
	$1f_{5/2}$	0	
	$1f_{7/2}$	0	
	$1h_{11/2}$	0	

2.7. Levels from the transfer reactions

Table 4 shows the results of the (d, p) and (d, t) measurements. In the first column the energy averaged over all spectra is given (for each angle a separate energy calibration has been performed). The columns four and five contain the assigned l and J values. If these values are given in brackets, the assignment is not sure. In the last two columns the spectroscopic values are given, obtained from direct comparison between the CHUCK3 output and the measured angular distribution.

Table 4
Spectroscopic information for ^{129}Te from (d, p) and (d, t)

E_x (keV)[a]	$(d\sigma/d\Omega)_{max}$, (μb/sr)[b]		Assignment[c]		Spectroscopic values	
(d, p), (d, t)	(d, p)	(d, t)	l	J^π	(d, p)[d], $10S_{lj}$	(d, t)[e], G_{lj}
0.0	2331	7269	2	$3/2^+$	3.3748	1.0816
105.2(4)	384	1340	5	$11/2^-$	1.8822	3.0195
179.35(28)	1021	7749	0	$1/2^+$	2.0163	0.5244
544.06(9)	34	67	2	$5/2^+$	0.0270	0.0070
633.51(7)	50		2	$3/2^+, 5/2^+$	0.0698	
760.25(5)	179	151	3	$7/2^-$	0.1240	0.0823
773.07(14)	40		0	$1/2^+$	0.0675	
812.93(8)	15	60	4	$7/2^+$	0.0763	0.0915
865.35(12)	8	16	(4)	$(7/2^+)$	(0.0276)	(0.0320)
874.73(21)	33	51	2	$3/2^+, 5/2^+$	0.0407	0.0055 0.0046
966.76(4)	405	3616	2	$5/2^+$	0.3411	0.3341
1162.14(15)	8		3	$5/2^-, 7/2^-$	0.0076	
1211.8(6)	33	365	4	$7/2^+$	0.1737	0.5373
1234.32(17)	7		2	$3/2^+, 5/2^+$	0.0082	
1282.0(5)	126	2047	2	$5/2^+$	0.1028	0.1762
1303.32(12)	55	55	0	$1/2^+$	0.1082	0.0023
1319.01(8)	4	15	4	$7/2^+$	0.0163	0.0212
1419.4(8)	30	442	2	$5/2^+$	0.0196	0.0346
1483.56(16)	5	66	4	$7/2^+$	0.0160	0.0905
1559.98(23)	12		1	$1/2^-, 3/2^-$	0.0196	
1582.1(4)	4	36	4	$7/2^+$	0.0105	0.0487
1599.65(20)	5	57	2	$5/2^+$	0.0034	0.0048
1655.72(22)	121	2204	2	$5/2^+$	0.0917	0.1688
1723.53(5)		46	2	$5/2^+$		0.0035
1739.72(11)		23	2	$3/2^+, 5/2^+$		0.0018 0.0015
1752.68(9)	146		3	$5/2^-, 7/2^-$	0.1286	
1754.24(9)		57	4	$7/2^+$		0.0838
1779.95(13)	35	559	2	$5/2^+$	0.0267	0.0405
1812.80(25)	9	37	4	$7/2^+$	0.0078	0.0501
1839.2(4)	6					
1843.64(15)		16	1+5			
1852.9(4)	5		3	$5/2^-, 7/2^-$	0.0564	
1869.57(6)	67		3	$5/2^-, 7/2^-$	0.0564	
1869.91(10)		320	2	$5/2^+$		0.0252
1887.52(25)		14	(1, 2)			
1918.7(5)		16	(2)	$(3/2^+)$		(0.0012)
1992.44(14)	8		(3)	$(5/2^-, 7/2^-)$	0.0062	
2040.2(6)	126 112	29	1	$3/2^-$	0.0790 0.0779	0.0006[f]
2059.31(9)		40	0	$1/2^+$		0.0013
2071.52(9)		40	2	$3/2^+$		0.0034

Table 4 (*continued*)

E_x (keV)[a]	$(d\sigma/d\Omega)_{max}$, (μb/sr)[b]		Assignment[c]		Spectroscopic values	
(d, p), (d, t)	(d, p)	(d, t)	l	J^π	(d, p)[d], $10S_{lj}$	(d, t)[e], G_{lj}
2072.43(11)	153 70		3	$7/2^-$	0.0855 0.0850	
2089.90(10)		9	(4)	$(7/2^+, 9/2^+)$		(0.0097 0.0062)
2106.60(7)	2146 995	55	3	$7/2^-$	1.1961 1.1836	0.0062[g]
2113.91(12)		112	0	$1/2^+$		0.0042
2132.69(11)	70 35		3	$7/2^-$	0.0355 0.0383	
2132.95(10)		11	5	$9/2^-, 11/2^-$		0.0314 0.0172
2141.81(15)		17	4	$7/2^+$		0.0233
2182.62(8)		40	2	$3/2^+$		0.0033
2197.7(5)		16	(3)	$(5/2^-, 7/2^-)$		(0.0073 0.0054)
2220.15(13)		31				
2221.28(8)	3009 1361		3	$7/2^-$	1.6872 1.6329	
2232.23(7)	362 188		3	$5/2^-, 7/2^-$	0.2859 0.3178	
2255.05(25)		65	0	$1/2^+$		0.0020
2266.61(19)		57	(2)	$(3/2^+)$		(0.0039)
2267.61(17)	156 134		1	$3/2^-$	0.1039 0.0984	
2278.52(13)		14	4	$(7/2^+)$		0.0166
2303.7(4)		12	5	$9/2^-, 11/2^-$		0.0368 0.0202
2312.17(12)	58 28		3	$7/2^-$	0.0325 0.0308	
2309.73(7)		86	0	$1/2^+$		0.0029
2316.60(12)		24	5	$(11/2^-)$		0.0405
2353.75(23)		199	0	$1/2^+$		0.0059
2360.05(6)	1302 1199		1	$3/2^-$	0.9215 0.9303	
2362.6(6)		28	1	$(1/2^-)$		0.0011
2370.5(5)		20	2	$(3/2^+)$		0.0015
2377.4(4)		24	1	$(1/2^-)$		0.0009
2379.95(8)	711 640		1	$3/2^-$	0.5006 0.5081	
2416.12(7)		94	2	$5/2^+$		0.0059
2427.21(13)	38 23		3	$7/2^-$	0.0213 0.0223	
2431.59(21)		22	0	$1/2^+$		0.0006
2454.28(13)		7	4	$7/2^+, 9/2^+$		0.0088 0.0057
2462.49(14)	62 36		3	$7/2^-$	0.0315 0.0347	
2465.29(23)		7	(2)	$(3/2^+, 5/2^+)$		(0.0006 0.0005)
2477.0(4)		15	(2)	$(3/2^+, 5/2^+)$		(0.0010 0.0008)
2481.62(29)		28	4	$7/2^+, 9/2^+$		0.0338 0.0221
2491.64(10)	27 27		1	$3/2^-$	0.0180 0.0214	
2506.66(13)		22	2	$(3/2^+)$		0.0018
2507.09(13)	27 24		(3)	$(5/2^-, 7/2^-)$	(0.0179 0.0270)	
2511.04(13)	35 18		(3)	$(5/2^-, 7/2^-)$	(0.0299 0.0270)	
2518.61(16)		23	2	$3/2^+$		0.0019
2524.39(32)	30 32		1	$1/2^-$	0.0445 0.0505	

Table 4 (*continued*)

E_x (keV)[a]	$(d\sigma/d\Omega)_{max}$, (μb/sr)[b]		Assignment[c]		Spectroscopic values	
(d, p), (d, t)	(d, p)	(d, t)	l	J^π	(d, p)[d], $10S_{lj}$	(d, t)[e], G_{lj}
2555.75(18)		45	2	$5/2^+$		0.0027
2581.14(9)	32 37		1	$3/2^-$	0.0268 0.0299	
2584.3(3)		14	2	$(3/2^+)$		0.0011
2612.43(10)	7 5		(3)	$(5/2^-, 7/2^-)$	(0.0055 0.0065)	
2615.91(13)		13	(2)	$(3/2^+, 5/2^+)$		(0.0009 0.0007)
2632.44(33)		22	2	$5/2^+$		0.0013
2641.3(4)	4 4		(3)	$(5/2^-, 7/2^-)$	(– 0.0050)	
2670.86(29)		5	(2)	$(3/2^+, 5/2^+)$		(0.0003 0.0003)
2680.6(4)		9	4	$9/2^+$		0.0062
2701.8(4)		11	1	$1/2^-$		0.0003
2705.76(6)	610 614		1	$1/2^-$	0.8145 0.9764	
2710.79(28)		34	2	$5/2^+$		0.0022
2728.21(10)	25 18		1	$1/2^-, 3/2^-$	0.0317 0.0318	
2736.55(15)	20 18		(1)	$(3/2^-)$	(0.0169 0.0126)	
2746.77(16)		42	2	$3/2^+, 5/2^+$		0.0028 0.0024
2756.74(9)		33	2	$(3/2^+)$		0.0024
2765.28(13)	33 8		(3)	$(5/2^-, 7/2^-)$	(0.0163 0.0154)	
2766.62(23)		19	2	$(5/2^+)$		0.0011
2811.67(7)	19 14		(5)	$(9/2^-, 11/2^-)$	(0.1061 0.1817)	
2819.45(12)	96 49		(3)	$(5/2^-, 7/2^-)$	(0.0613 0.0617)	
2823.60(24)		18	4	$7/2^+, 9/2^+$		0.0193 0.0123
2831.1(6)		12	(2)	$(3/2^+)$		(0.0009)
2835.22(13)	56 27		(3)	$(5/2^-, 7/2^-)$	(0.0368 0.0378)	
2844.1(5)		6	2	$3/2^+, 5/2^+$		0.0005 0.0004
2853.69(7)	102 49		(3)	$(5/2^-, 7/2^-)$	(0.0684 0.0676)	
2855.67(12)		36	2	$5/2^+$		0.0023
2859.54(11)	39 16		(3)	$(5/2^-, 7/2^-)$	(0.0223 0.0219)	
2871.21(7)	73 36		(3)	$(5/2^-)$	(0.0482 0.0493)	
2889.84(9)	44 26		(3)	$(5/2^-, 7/2^-)$	(0.0310 0.0291)	
2899.90(17)	16 5		5	$9/2^-, 11/2^-$	0.0442 0.0771	
2919.63(9)	103 50		3	$(5/2^-)$	0.0689 0.0704	
2971.34(10)	62 28		3	$7/2^-$	0.0296 0.0239	
2979.44(6)	713 353		3	$5/2^-$	0.4617 0.4705	
2999.62(27)	6					
3009.43(9)	7					
3023.78(26)	3					
3029.07(8)	23					
3046.25(8)	15					
3056.36(13)	6					
3070.43(3)	6					

Table 4 (*continued*)

E_x (keV)[a]	$(d\sigma/d\Omega)_{max}$, (μb/sr)[b]		Assignment[c]		Spectroscopic values	
(d, p), (d, t)	(d, p)	(d, t)	l	J^π	(d, p)[d], $10S_{lj}$	(d, t)[e], G_{lj}
3089.26(9)	48					
3102.75(9)	40					
3128.47(29)	10					
3133.45(6)	35					
3150.71(10)	16					
3163.3(4)	3					
3182.02(18)	15					
3202.32(26)	7					
3211.79(29)	4					
3230.49(13)	61					
3246.07(11)	58					
3253.08(10)	23					
3260.88(22)	10					
3277.1(5)	12					
3281.58(18)	38					
3295.7(5)	3					
3306.39(11)	15					
3321.35(12)	34					
3326.60(18)	9					
3350.26(17)	7					
3355.63(10)	27		1	$3/2^-$	0.0197	
3361.46(10)	48					
3364.58(9)	98					
3371.62(10)	37					
3379.29(9)	14					
3384.75(8)	92					
3389.76(29)	12					
3405.79(10)	46					
3414.31(15)	27					
3419.88(12)	76					
3428.91(10)	105		1	$(3/2^-)$	0.1082	
3441.00(9)	87					
3452.75(14)	9					
3461.13(8)	126					
3474.79(13)	66					
3479.09(21)	32					
3489.57(14)	19		1	$1/2^-$	0.0307	
3503.37(9)	202		(1)	$(3/2^-)$	(0.1849)	
3511.99(8)	73					
3524.24(15)	36					
3527.74(9)	46		(1)	$(1/2^-)$	(0.0741)	

Table 4 (*continued*)

E_x (keV)[a]	$(d\sigma/d\Omega)_{max}$, (μb/sr)[b]		Assignment[c]		Spectroscopic values	
(d, p), (d, t)	(d, p)	(d, t)	l	J^π	(d, p)[d], $10S_{lj}$	(d, t)[e], G_{lj}
3545.82(7)	102		(1)	$(3/2^-)$	(0.0960)	
3559.29(10)	19					
3564.98(10)	80		1	$1/2^-$	0.1221	
3569.24(10)	53					
3579.66(15)	9					
3587.43(6)	176					
3593.73(17)	20					
3600.49(7)	30		1	$(3/2^-)$	0.0271	
3615.20(7)	77					
3622.88(26)	5					
3628.68(29)	5					
3634.19(8)	57					
3638.44(6)	77		1	$1/2^-$	0.1325	
3643.26(5)	56					
3648.97(9)	57		1	$1/2^-$	0.0953	
3655.05(10)	108					
3666.42(19)	6					
3671.50(11)	19		1	$3/2^-$	0.0193	
3677.85(6)	62					
3695.69(8)	147					
3707.67(13)	58		1	$1/2^-$	0.1028	
3713.78(22)	19					
3729.32(19)	21					
3737.13(8)	39					
3744.94(9)	39		1	$3/2^-$	0.0329	
3752.27(18)	16					
3764.98(9)	36		1	$(3/2^-)$	0.0336	
3769.94(6)	49					
3777.52(14)	30					
3784.59(7)	28					
3792.58(6)	460		1	$3/2^-$	0.4014	
3800.93(16)	24					
3811.7(4)	9					
3818.90(11)	18					
3826.71(11)	11					
3837.66(6)	38					
3851.94(8)	35		1	$3/2^-$	0.0329	
3859.62(20)	9					
3865.73(4)	95		1	$3/2^-$	0.0829	
3873.38(10)	182					
3884.50(16)	16					

Table 4 (*continued*)

E_x (keV)[a]	$(d\sigma/d\Omega)_{max}$, (μb/sr)[b]		Assignment[c]		Spectroscopic values	
(d, p), (d, t)	(d, p)	(d, t)	l	J^π	(d, p)[d], $10S_{lj}$	(d, t)[e], G_{lj}
3890.23(13)	165					
3899.34(9)	51		1	$3/2^-$	0.0462	
3906.92(5)	66					
3917.0(4)	11					
3921.60(10)	24					
3929.44(23)	6					
3938.45(12)	51					
3944.24(16)	31					
3948.09(24)	22		(1)	$(3/2^-)$	(0.0201)	
3952.81(16)	48					
3962.33(15)	12					
3969.35(29)	20		(1)	$(3/2^-)$	(0.0214)	
3974.29(10)	95		1	$3/2^-$	0.0858	
3986.75(26)	6					
3993.70(17)	21					
3997.60(14)	32					
4002.40(28)	28					
4005.76(24)	48					
4017.11(11)	42					
4024.93(14)	31					
4032.54(10)	37		1	$3/2^-$	0.0380	
4043.32(12)	24					
4045.78(16)	52					
4053.70(20)	22					
4059.09(9)	44		1	$(1/2^-)$	0.0816	
4067.78(8)	88		1	$3/2^-$	0.0875	
4072.22(21)	36					
4082.23(13)	48		1	$3/2^-$	0.0484	
4086.77(9)	99		1	$3/2^-$	0.0919	
4092.48(28)	13					
4101.8(4)	16					
4106.1(4)	31					
4110.4(4)	32					
4122.07(10)	90		1	$1/2^-$	0.1548	
4128.98(12)	41					
4132.81(15)	133		1	$3/2^-$	0.1314	
4150.2(4)	5					
4161.1(5)	8					
4166.21(10)	47					
4175.10(19)	33		1	$(1/2^-)$	0.0569	
4181.18(9)	70		1	$(3/2^-)$	0.0687	

Table 4 (*continued*)

E_x (keV)[a]	$(d\sigma/d\Omega)_{max}$, (μb/sr)[b]		Assignment[c]		Spectroscopic values	
(d, p), (d, t)	(d, p)	(d, t)	l	J^π	(d, p)[d], $10S_{lj}$	(d, t)[e], G_{lj}
4200.84(12)	59					
4205.89(6)	47		1	$1/2^-$	0.1038	
4212.43(12)	25					
4220.07(19)	85		1	$3/2^-$	0.0811	
4229.10(14)	38					
4239.79(9)	73		1	$3/2^-$	0.0729	
4251.2(4)	23					
4259.33(23)	25					
4267.41(15)	19		1	$(1/2^-)$	0.0330	
4277.37(10)	105		1	$3/2^-$	0.0912	
4291.21(29)	11					
4298.46(22)	42		1	$1/2^-$	0.0737	
4306.73(19)	18					
4311.74(9)	53		1	$(1/2^-)$	0.0956	
4317.05(13)	19					
4326.49(8)	85					
4336.16(19)	32		1	$(1/2^-)$	0.0628	
4349.48(12)	43					
4356.27(9)	105		1	$1/2^-$	0.2097	
4365.34(11)	238		1	$1/2^-$	0.4293	
4372.60(17)	99					
4380.55(12)	65					
4389.09(20)	168		1	$1/2^-$	0.3284	
4402.14(22)	47					
4410.53(17)	59					
4425.13(10)	65		(1)	$(3/2^-)$	(0.0524)	
4433.07(10)	123		1	$3/2^-$	0.1380	
4444.04(15)	67					
4456.37(12)	81					
4467.43(15)	106		(1)	$(1/2^-)$	(0.2381)	
4474.7(4)	62					
4483.92(16)	99					
4496.75(15)	76					
4504.21(17)	40					
4511.76(22)	28					
4522.5(5)	53					
4543.28(25)	41					
4558.21(29)	77					
4572.69(21)	64					
4580.26(23)	62					
4589.16(25)	126					
4595.2(5)	67					
4608.4(4)	71					

Table 4 (*continued*)

E_x (keV)[a]	$(d\sigma/d\Omega)_{max}$, (μb/sr)[b]		Assignment[c]		Spectroscopic values	
(d, p), (d, t)	(d, p)	(d, t)	l	J^π	(d, p)[d], $10S_{lj}$	(d, t)[e], G_{lj}
4621.96(21)	52					
4634.7(5)	30					
4643.2(4)	47		(1)	$(1/2^-, 3/2^-)$	(0.0986)	
4652.9(4)	42		(1)	$(1/2^-, 3/2^-)$	(0.0657)	
4665.82(18)	39		1	$1/2^-, 3/2^-$	0.0815	
4682.0(3)	20		1	$1/2^-, 3/2^-$	0.0398	
4695.4(5)	21					
4711.80(25)	30		1			
4724.34(20)	32					
4743.5(4)	55					
4766.2(5)	18					
4777.9(4)	27		(1)	$(1/2^-, 3/2^-)$	(0.0401)	
4794.33(24)	42					
4807.86(29)	33					
4840.4(4)	112					
4849.6(6)	18					
4868.2(5)	57					
4879.66(24)	38					
4907.4(5)	96					
4917.0(5)	86		(1)	$(1/2^-, 3/2^-)$	(0.1291)	
4929.4(5)	112					
4946.8(4)	68					
4958.3(3)	88					
4975.3(4)	56					
5002.3(4)	44					
5013.3(7)	44					

[a] The energies are weighted means of the (d, p) and (d, t) measurements, if the level was seen in both reactions. For (d, p) energies up to 2379 keV (incl.) the values of the measurement at $E_d = 24$ MeV are given, above these of the measurement at $E_d = 18$ MeV. The energy values of the single measurements are mean energies of all angles. The error given here is only the statistical error (cf. Table 6).

[b] In each case the maximum value of the angular distribution is given. In the region where the (d, p) measurements overlap the upper value is the maximum at $E_d = 24$ MeV, the lower one the maximum at $E_d = 18$ MeV, respectively.

[c] The assignment of the l values was done via the angular distributions of the cross section, the assignment of the J values via the angular distributions of the analyzing power in $(\vec{d}, t)$. The identification of J at levels from (d, p) was done via the polarized measurement at 22°, but only for levels with $l = 1$, $l = (1)$ and $l = 3$. Above 3 MeV an l value was only assigned to levels with $l = 1$ or $l = (1)$. No information from (n, $\gamma\gamma$) was used.

[d] For levels with ambiguous J assignment $10S_{lj}$ for the smaller J value is given. The ratios of S_{lj} for its determination for the larger value (respectively) are: $1/2^- : 3/2^- = 2.0$, $3/2^+ : 5/2^+ = 1.65$, $5/2^- : 7/2^- = 1.55$, $7/2^+ : 9/2^+ = 1.85$, and $9/2^- : 11/2^- = 1.9$ (about 5% error). In the region where the (d, p) measurements overlap the upper value belongs to the measurement at $E_d = 24$ MeV and the lower one to $E_d = 18$ MeV, respectively.

[e] For levels with ambiguous J the upper number belongs to the smaller J value and the lower one to the larger J value, respectively.

[f] Adopted configuration $\nu 3p3/2^-$.

[g] Adopted configuration $\nu 2f7/2^-$.

By fitting the potential parameters of the DWBA calculations the (d, p) spectroscopic factors of the ground state and the first two excited states have been adjusted to earlier stripping reactions [19,21]. The (d, p) measurement at $E_d = 18$ MeV has been adjusted to the measurement at $E_d = 24$ MeV. This causes the good agreement of the spectroscopic factors in the overlapping region. The cross sections make clear, that the lower beam energy leads to an enhancement of the levels with $l = 1$. The cross sections for levels with $l = 3$ are drastically lower, for example, while they stay nearly the same for levels with $l = 1$.

In the analysis of the (d, t) measurement the DWBA parameters were not adjusted to former pickup reactions. Therefore, the spectroscopic factors came out a factor of about two smaller than in Refs. [18,38].

3. Level scheme

The results of the (n, $\gamma\gamma$) measurement at Řež and of the transfer reactions at Munich were put together to construct a detailed level scheme of ^{129}Te. All levels populated in the (n, $\gamma\gamma$) measurement are given in Table 5. The known level scheme of ^{129}Te [22] was the starting point. With the help of the $\gamma\gamma$ coincidences the level scheme was expanded under following conditions:

(i) confirmation of the new level by several independent coincidences, or
(ii) population of the level in a transfer reaction and existence of at least one deexciting line confirmed by $\gamma\gamma$ coincidences.

The energies of the levels have been determined with the program LEVFIT [39] which calculates the position of the levels with a least squares fit procedure to the transition energies. In this way the neutron separation energy has been determined to be (6082.42 ± 0.03) keV, where a systematic error of about 80 eV has to be added because of the energy calibration of the single spectra.

Spin-parity assignments have been made with the help of all existing data. Main criteria from (n, $\gamma\gamma$) were:

(i) for levels fed by a primary transition J^π was assumed to be $1/2^\pm$ or $3/2^\pm$, and
(ii) only transitions with multipolarities E1, M1 and E2 have been assumed.

Fig. 8 shows the first 17 levels from (n, $\gamma\gamma$) and their decay. The level at 773.2 keV that had not been observed in earlier studies [26] is the second $1/2^+$ state. This level has also been seen in the (d, p) measurement for the first time. The intensity of the twice placed γ line with 773.2 keV that depletes also the level at 1317.8 keV was divided with the help of coincidence spectra. The new $5/2^-$ state at 1221.3 keV is depopulated by the intense 756.6 keV γ line to the $9/2^-$ state at 464.6 keV. Formerly, this line was supposed to depopulate a possible $1/2_2^+$ state at 937 keV or 756 keV [26,40]. The level at 1221.3 keV has turned out to be a strong gateway in the population of the $11/2^-$ isomer through the level at 464.6 keV [11].

Table 5
Gamma decay of the levels from (n, $\gamma\gamma$). The energies E_{trans} are the recoil-corrected γ energies (cp. Table 1). E_{i} and E_{f} are the energies of the initial and the final level of the transition, respectively

E_{i} (keV)	J^{π}	E_{trans} (keV)	I_{γ} (%)	E_{f} (keV)	J^{π}
180.37(3)	1/2+	180.3	44.03	0.0	3/2+
464.63(4)	9/2−	359.2	7.60	105.5	11/2−
544.60(3)	5/2+	544.6	5.37	0.0	3/2+
		364.3	0.15	180.4	1/2+
633.75(3)	3/2+	633.8	3.92	0.0	3/2+
		453.3	1.01	180.4	1/2+
759.82(4)	7/2−	654.3	2.85	105.5	11/2−
		295.3	1.23	464.6	9/2−
773.21(3)	1/2+	773.2[a]	2.79	0.0	3/2+
		592.8	0.89	180.4	1/2+
812.93(7)	7/2+	812.9	0.54	0.0	3/2+
874.88(4)	3/2+	874.8	3.18	0.0	3/2+
		694.5	2.17	180.4	1/2+
		330.3	1.10	544.6	5/2+
966.84(5)	5/2+	966.9	1.25	0.0	3/2+
		786.5[ab]	0.42	180.4	1/2+
1162.21(8)	7/2−	1056.5	0.21	105.5	11/2−
		697.6	2.67	464.6	9/2−
1221.26(4)	5/2−	1221.2	0.13	0.0	3/2+
		756.6	3.08	464.6	9/2−
		461.5	0.65	759.8	7/2−
1233.82(8)	3/2+, 5/2+	1053.4	0.36	180.4	1/2+
		689.2[a]	0.40	544.6	5/2+
1281.57(6)	5/2+	1281.6	0.39	0.0	3/2+
		736.9	0.38	544.6	5/2+
1303.41(7)	1/2+	1303.6	0.23	0.0	3/2+
		1123.0	0.57	180.4	1/2+
		669.6	0.25	633.8	3/2+
1317.83(8)	7/2+	1318.5	0.16	0.0	3/2+
		773.2[a]	0.10	544.6	5/2+
		684.6	0.17	633.8	3/2+
1421.34(9)	5/2+	1421.4	0.48	0.0	3/2+
		648.1	0.19	773.2	1/2+
1559.85(5)	3/2−	1559.7	0.39	0.0	3/2+
		1379.3	0.18	180.4	1/2+
		800.0	0.63	759.8	7/2−
		786.5[a]	0.42	773.2	1/2+
		338.7	0.45	1221.3	5/2−
1599.38(10)	5/2+	786.5[a]	0.42	812.9	7/2+
1656.26(8)	5/2+	1656.3	0.52	0.0	3/2+
1752.30(7)	5/2−	1752.7	0.17	0.0	3/2+
		1287.6	0.20	464.6	9/2−
		992.5	0.43	759.8	7/2−
		590.0	0.20	1162.2	7/2−
1851.55(7)	5/2−	1851.3	0.37	0.0	3/2+
		1091.4	0.14	759.8	7/2−
		885.1	0.11	966.8	5/2+
		689.2[a]	1.41	1162.2	7/2−
1868.88(18)	5/2+	1324.7	0.21	544.6	5/2+

Table 5 (*continued*)

E_i (keV)	J^π	E_{trans} (keV)	I_γ (%)	E_f (keV)	J^π
		1234.6	0.26	633.8	3/2+
		1095.5	0.26	773.2	1/2+
2040.19(6)	3/2−	2040.4	0.71	0.0	3/2+
		1859.7	1.51	180.4	1/2+
		818.9	0.43	1221.3	5/2−
		480.2	0.28	1559.9	3/2−
2221.66(8)	(3/2+), 3/2−	2221.5	0.98	0.0	3/2+
		2041.7	0.34	180.4	1/2+
		1677.3	0.48	544.6	5/2+
		1000.3	0.34	1221.3	5/2−
2267.24(6)	3/2−	2267.2	0.12	0.0	3/2+
		2086.9	1.32	180.4	1/2+
		1633.6	0.26	633.8	3/2+
		1493.9[a]	0.29	773.2	1/2+
		1105.5	0.20	1162.2	7/2−
		1045.8	0.36	1221.3	5/2−
		707.2	0.41	1559.9	3/2−
2360.49(3)	3/2−	2360.4	3.22	0.0	3/2+
		2180.1	17.22	180.4	1/2+
		1815.6	0.08	544.6	5/2+
		1586.8	0.14	773.2	1/2+
		1485.5	0.33	874.9	3/2+
		1139.2	0.39	1221.3	5/2−
		800.4	0.48	1559.9	3/2−
		704.4	0.14	1656.3	5/2+
2379.57(3)	3/2−	2379.5	2.06	0.0	3/2+
		2199.2	5.70	180.4	1/2+
		1834.9	0.26	544.6	5/2+
		1745.8	0.24	633.8	3/2+
		1619.5	0.34	759.8	7/2−
		1606.6	0.60	773.2	1/2+
		1504.4	0.57	874.9	3/2+
		1412.5	0.08	966.8	5/2+
		1158.4	0.83	1221.3	5/2−
		1097.9	0.49	1281.6	5/2+
		723.2	0.11	1656.3	5/2+
		527.9	0.22	1851.6	5/2−
2493.07(10)	3/2−	2493.2	0.14	0.0	3/2+
		2312.7	0.12	180.4	1/2+
		1526.5	0.11	966.8	5/2+
		641.8	0.11	1851.6	5/2−
		623.9	0.09	1868.9	5/2+
2524.76(7)	1/2−	2524.8[a]	1.08	0.0	3/2+
		2343.8	0.19	180.4	1/2+
		1649.5[a]	0.31	874.9	3/2+
2581.69(9)	3/2−	2581.6	0.09	0.0	3/2+
		2401.8	0.27	180.4	1/2+
		1360.5	0.17	1221.3	5/2−
		730.0	0.19	1851.6	5/2−
2705.13(3)	1/2−	2705.1	3.23	0.0	3/2+
		2524.8[a]	4.78	180.4	1/2+

Table 5 (*continued*)

E_i (keV)	J^π	E_{trans} (keV)	I_γ (%)	E_f (keV)	J^π
		2071.1	0.43	633.8	3/2+
		1931.9	0.31	773.2	1/2+
		1830.2	2.12	874.9	3/2+
		1471.0	0.27	1233.8	3/2+, 5/2+
		1401.4	0.13	1303.4	1/2+
		437.5	0.07	2267.2	3/2−
		344.6	0.22	2360.5	3/2−
3355.48(19)	3/2−	3355.2	0.73	0.0	3/2+
3429.8(3)	3/2−	3250.1	0.10	180.4	1/2+
		2670.5	0.11	759.8	7/2−
		2554.1	0.26	874.9	3/2+
3502.59(7)	3/2−	3322.1	0.28	180.4	1/2+
		2741.5	0.07	759.8	7/2−
		2627.8	0.12	874.9	3/2+
3528.30(14)	(1/2−)	3528.5	0.54	0.0	3/2+
		3348.7	0.64	180.4	1/2+
		2754.9	0.14	773.2	1/2+
		2652.4[a]	0.19	874.9	3/2+
3546.92(9)	(3/2−)	3546.7	0.05	0.0	3/2+
		3366.4	0.22	180.4	1/2+
		1987.6	0.05	1559.9	3/2−
3564.51(16)	1/2−	3564.8	1.04	0.0	3/2+
3638.38(6)	1/2−	3638.4	0.69	0.0	3/2+
		3457.7	0.33	180.4	1/2+
3648.77(11)	1/2−	3468.8	0.39	180.4	1/2+
3792.41(4)	3/2−	3792.5	0.39	0.0	3/2+
		3612.1	2.14	180.4	1/2+
		3018.8	0.11	773.2	1/2+
		2371.1	0.11	1421.3	5/2+
3852.72(12)	3/2−	3672.3	0.26	180.4	1/2+
		2630.1	0.08	1221.3	5/2−
3865.37(10)	3/2−	3684.8	0.55	180.4	1/2+
4032.6(3)	3/2−	3853.7	0.50	180.4	1/2+
4087.57(12)	3/2−	3907.3	0.25	180.4	1/2+
		1708.4[a]	0.50	2379.6	3/2−
4121.20(9)	1/2−	4120.6	0.06	0.0	3/2+
		3940.5	0.24	180.4	1/2+
4133.52(9)	3/2−	4133.3	0.46	0.0	3/2+
		3952.9	0.26	180.4	1/2+
4175.2(3)	(1/2−)	4174.7	0.32	0.0	3/2+
4180.7(3)	(3/2−)	4001.6	0.22	180.4	1/2+
4204.2(3)	1/2−	4204.2	0.21	0.0	3/2+
4220.59(22)	3/2−	1999.6	0.24	2221.7	(3/2+), 3/2−
		427.7	0.05	3792.4	3/2−
4240.5(3)	3/2−	4060.6	0.21	180.4	1/2+
4277.03(11)	3/2−	4096.6	0.10	180.4	1/2+
4297.82(21)	1/2−	4297.8	0.17	0.0	3/2+
4356.15(13)	(1/2−)	4174.7	0.32	180.4	1/2+
4364.58(5)	1/2−	4364.5	0.83	0.0	3/2+
		4184.1	0.44	180.4	1/2+
4374.0(3)	(1/2−, 3/2−)	4374.7	0.07	0.0	3/2+

Table 5 (*continued*)

E_i (keV)	J^π	E_{trans} (keV)	I_γ (%)	E_f (keV)	J^π
4388.95(10)	1/2−	4208.5	0.44	180.4	1/2+
4432.94(10)	3/2−	4433.7	0.65	0.0	3/2+
		4252.1	0.23	180.4	1/2+
4588.50(12)	(1/2−, 3/2−)	4588.7	0.21	0.0	3/2+
6082.42(3)	1/2+	6082.2	0.39	0.0	3/2+
		5901.7	0.59	180.4	1/2+
		5449.5	0.22	633.8	3/2+
		4523.1	0.23	1559.9	3/2−
		4426.9	0.23	1656.3	5/2+
		4042.2	2.09	2040.2	3/2−
		3860.7	1.00	2221.7	(3/2+), 3/2−
		3815.2	2.39	2267.2	3/2−
		3721.9	19.54	2360.5	3/2−
		3702.9	10.33	2379.6	3/2−
		3589.5	0.52	2493.1	3/2−
		3557.7	1.16	2524.8	1/2−
		3500.6	0.86	2581.7	3/2−
		3377.3	10.44	2705.1	1/2−
		2726.7	0.68	3355.5	3/2−
		2652.4[a]	0.65	3429.8	3/2−
		2579.8	1.06	3502.6	3/2−
		2554.1	0.43	3528.3	(1/2−)
		2535.5	0.79	3546.9	(3/2−)
		2518.1	1.14	3564.5	1/2−
		2444.0	0.97	3638.4	1/2−
		2433.7	0.56	3648.8	1/2−
		2290.0	3.83	3792.4	3/2−
		2229.7	0.53	3852.7	3/2−
		2217.0	0.85	3865.4	3/2−
		2049.9	0.51	4032.6	3/2−
		1994.9	0.68	4087.6	3/2−
		1961.2	0.63	4121.2	1/2−
		1948.8	0.61	4133.5	3/2−
		1907.0	0.20	4175.2	(1/2−)
		1901.8	0.34	4180.7	(3/2−)
		1878.2	0.28	4204.2	1/2−
		1861.8	0.58	4220.6	3/2−
		1842.1	0.49	4240.5	3/2−
		1805.4	0.40	4277.0	3/2−
		1784.6	0.22	4297.8	1/2−
		1726.3	0.28	4356.2	(1/2−)
		1717.8	1.76	4364.6	1/2−
		1708.4[a]	0.50	4374.0	(1/2−, 3/2−)
		1693.5	0.93	4389.0	1/2−
		1649.5[a]	0.48	4432.9	3/2−
		1493.9[a]	0.45	4588.5	(1/2−, 3/2−)

[a] Multiply placed, see Table 1.
[b] Placement not confirmed by coincidences.

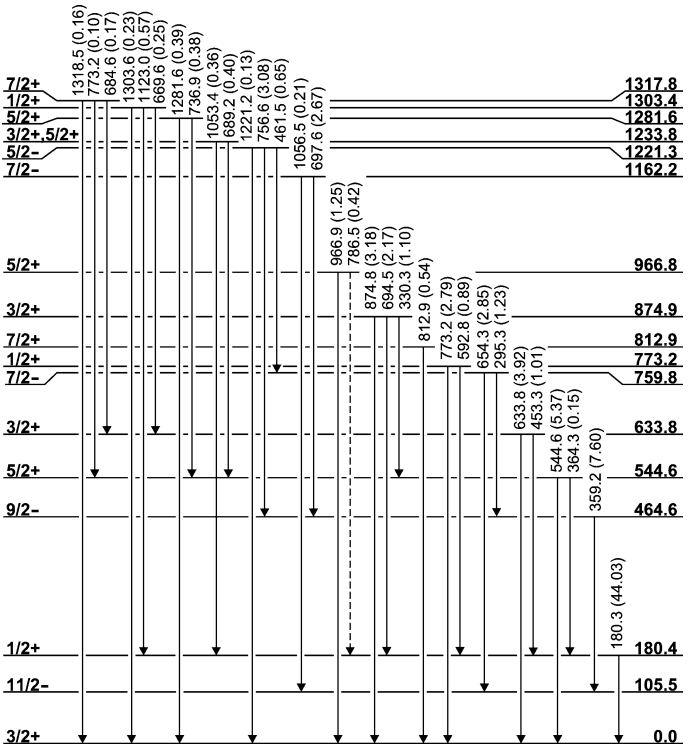

Fig. 8. The first 17 levels of ^{129}Te and their decay.

Two lines that have been seen in coincidence with each other and in coincidence with the 698 keV line shall be mentioned here. According to Table 1 and Fig. 2, the careful reader may propose that the γ lines 301 keV and 916 keV could be combined to a level at 1463 keV or 2078 keV, if one of them feeds the 1162 keV level directly and the other one is placed above. The chain of both would than deexcite the level at 2380 keV. Unfortunately, none of these possible levels at 1463 keV or 2078 keV could be confirmed, neither with independent coincidences, nor through the transfer reactions. This is why a placement of the γ lines 301 keV and 916 keV was not possible.

Finally, in Table 6 the whole experimental level scheme of ^{129}Te is presented as it was obtained from a combination of the performed $(\mathrm{n}, \gamma\gamma)$ and transfer reactions. Already below 1 MeV excitation energy the comparison with the levels known so far from β^- decay and other studies [22] is interesting. We did not observe the levels at 245 keV, 360 keV and 455 keV. Their existence is questionable, because they are most probably based on background in earlier neutron pickup reactions. Also the level at 775(5) keV listed in the Nuclear Data Sheets from an earlier (p, d) and $(^3\mathrm{He}, \alpha)$ measurement [18] is probably not existing, because it was not seen in our $(\vec{\mathrm{d}}, \mathrm{t})$ measurement. The same is valid for the 819 keV level. Because of the separation of the closely lying levels at 865 keV and 875 keV in the transfer reactions the situation around this energy could be cleared. In

Table 6
Level scheme of ^{129}Te from (n, $\gamma\gamma$), (d, p) and (d, t)

This work				Other works				Adopted levels	
Level energy E_x (keV)[a]			l	(d, p)[b]		(p, d)[c]	(d, t)[d]		
(n, $\gamma\gamma$)	(d, p)	(d, t)		E_x	l	E_x	E_x	E_x (keV)[e]	J^π
0	0	0	2	0	2	0	0	0	3/2+
105.51(5)	105.2(4)	106	5	106	5	107	0.10	105.51(5)	11/2−
180.37(3)	179.4(3)	180	0	179	0	181	0.18	180.37(3)	1/2+
						250	0.25	–[f]	
						360	0.36	–[f]	
						455	0.42	–[f]	
464.63(4)								464.63(4)	9/2−
544.60(3)	544.1(3)	545	2	542		539	0.55	544.60(3)	5/2+
633.75(3)	633.5(3)		2	635				633.75(3)	3/2+
759.82(4)	760.3(3)	760.2(3)	3	763		775	0.73	759.82(4)	7/2−
773.21(3)	773.1(3)		0					773.21(3)	1/2+
812.93(7)	813.0(3)	812.9(3)	4			819	0.80	812.93(7)	7/2+
	865.5(3)	865.2(3)	(4)					865.4(6)	(7/2+)
874.88(4)	874.6(3)	875.1(3)	2	878		872	0.87	874.88(4)	3/2+
966.84(5)	966.8(3)	966.7(3)	2	967	2	971	0.96	966.84(5)	5/2+
1162.21(8)	1162.1(3)		3					1162.21(8)	7/2−
	1212.7(3)	1211.5(3)	4			1217		1211.8(8)	7/2+
1221.26(4)								1221.26(4)	5/2−
1233.82(8)	1234.3(3)		2					1233.82(8)	3/2+, 5/2+
1281.57(6)	1281.4(3)	1282.4(3)	2	1284		1290	1.27	1281.57(6)	5/2+
1303.41(7)	1303.5(3)	1303.2(3)	0	1306				1303.41(7)	1/2+
1317.83(8)	1319.2(3)	1319.0(3)	4					1317.83(8)	7/2+
1421.34(9)	1420.4(3)	1418.8(3)	2			1430		1421.34(9)	5/2+
	1483.1(5)	1483.6(3)	4			1490		1483.6(6)	7/2+
1559.85(5)	1560.0(3)		1					1559.85(5)	3/2−
	1579.9(4)	1582.1(3)	4					1582.1(7)	7/2+
1599.38(10)	1599.1(3)	1599.7(3)	2					1599.38(10)	5/2+
1656.26(8)	1655.5(3)	1656.0(3)	2	1654		1672	1.64	1656.26(8)	5/2+
		1723.5(3)	2					1723.5(6)	5/2+
		1739.7(3)	2					1739.7(6)	3/2+, 5/2+
1752.30(7)	1752.7(3)		3	1753				1752.30(7)	5/2−
		1754.2(3)	4					1754.2(5)	7/2+
	1780.1(3)	1779.9(3)	2	1776		1797	1.76	1780.0(6)	5/2+
	1813.4(3)	1812.7(3)	4					1812.8(6)	7/2+
	1839.2(4)							1839.2(7)	
		1843.6(3)	1 + 5					1843.6(6)	
1851.55(7)	1852.9(4)		3					1851.55(7)	5/2−
1868.88(18)		1869.9(3)	2			1892		1868.88(18)	5/2+
	1869.6(3)		3	1869				1869.6(6)	5/2−, 7/2−
		1887.5(3)	(1,2)					1887.5(6)	
		1918.7(5)	(2)					1918.7(8)	(3/2+)
	1992.4(3)		(3)					1992.4(6)	(5/2−, 7/2−)
2040.19(6)	2040.3(3)	2038.4(3)	1	2040				2040.19(6)	3/2−
		2059.3(3)	0					2059.3(10)	1/2+
		2071.5(3)	2					2071.5(10)	3/2+

Table 6 (*continued*)

This work				Other works				Adopted levels	
Level energy E_x (keV)[a]			l	(d, p)[b]		(p, d)[c]	(d, t)[d]		
(n, $\gamma\gamma$)	(d, p)	(d, t)		E_x	l	E_x	E_x	E_x (keV)[e]	J^π
	2072.4(3)		3	2071				2072.4(6)	7/2−
		2089.9(3)	(4)					2089.9(10)	(7/2+, 9/2+)
	2106.6(3)	2106.6(3)	3	2106	3			2106.6(6)	7/2−
		2113.9(3)	0			2140	2.09	2113.9(10)	1/2+
	2132.7(3)		3	2135				2132.7(6)	5/2−, 7/2−
		2133.0(3)	5					2133.0(10)	9/2−, 11/2−
		2141.8(3)	4					2141.8(10)	7/2+
		2182.6(3)	2					2182.6(10)	3/2+
		2197.7(5)	(3)					2197.7(10)	(5/2−, 7/2−)
		2220.2(3)						2220.2(10)	
	2221.3(3)		3	2221	3			2221.3(6)	7/2−
2221.66(8)								2221.66(8)	3/2−
	2232.2(3)		3					2232.2(6)	(5/2−, 7/2−)
		2255.1(3)	0				2.24	2255.1(15)	1/2+
		2266.6(3)	(2)					2266.6(15)	(3/2+)
2267.24(6)	2267.6(3)		1	2261	1			2267.24(6)	3/2−
		2278.5(3)	4					2278.5(15)	(7/2+)
		2303.7(4)	5					2303.7(15)	9/2−, 11/2−
		2309.7(3)	0					2309.7(15)	1/2+
	2312.2(3)		3	2314				2312.2(6)	7/2−
		2316.6(3)	5					2316.6(15)	(11/2−)
		2353.8(3)	0			2370	2.34	2353.8(15)	1/2+
2360.49(3)	2360.1(3)		1	2360	1			2360.49(3)	3/2−
		2362.6(6)	1					2362.6(15)	(1/2−)
		2370.5(5)	2					2370.5(15)	(3/2+)
		2377.4(4)	1					2377.4(15)	(1/2−)
2379.57(3)	2380.0(3)		1	2379	1			2379.57(3)	3/2−
		2416.1(3)	2			2450		2416.1(20)	5/2+
	2427.2(3)		3					2427.2(6)	7/2−
		2431.6(3)	0					2431.6(20)	1/2+
		2454.3(3)	4					2454.3(20)	7/2+, 9/2+
	2462.5(3)		3					2462.5(6)	7/2−
		2465.3(3)	(2)					2465.3(20)	(3/2+, 5/2+)
		2477.0(4)	(2)					2477.0(20)	(3/2+, 5/2+)
		2481.6(3)	4					2481.6(20)	7/2+, 9/2+
2493.07(10)	2491.6(3)		1	2491				2493.07(10)	3/2−
		2506.7(3)	2					2506.7(29)	(3/2+)
	2507.1(3)		(3)					2507.1(6)	(5/2−, 7/2−)
	2511.0(3)		(3)					2511.0(6)	(5/2−, 7/2−)
		2518.6(3)	2					2518.6(29)	3/2+
2524.76(7)	2524.4(3)		1					2524.76(7)	1/2−
		2555.8(3)	2					2555.8(29)	5/2+
2581.69(9)	2581.1(3)		1	2578				2581.69(9)	3/2−
		2584.3(3)	2					2584.3(29)	(3/2+)
	2612.4(3)		(3)					2612.4(6)	(5/2−, 7/2−)
		2615.9(3)	(2)					2615.9(29)	(3/2+, 5/2+)
		2632.4(4)	2					2632.4(29)	5/2+

Table 6 (*continued*)

This work				Other works				Adopted levels	
Level energy E_x (keV)[a]			l	(d, p)[b]		(p, d)[c]	(d, t)[d]		
(n, $\gamma\gamma$)	(d, p)	(d, t)		E_x	l	E_x	E_x	E_x (keV)[e]	J^π
	2641.3(4)		(3)					2641.3(7)	(5/2−, 7/2−)
		2670.9(3)	(2)					2671(4)	(3/2+, 5/2+)
		2680.6(4)	4					2681(4)	9/2+
		2701.8(4)	1					2702(4)	(1/2−)
2705.13(3)	2705.8(3)		1	2704	1			2705.13(3)	1/2−
		2710.8(3)	2					2711(4)	5/2+
	2728.2(3)		1					2728.2(6)	1/2−, 3/2−
	2736.6(3)		(1)					2736.6(6)	(3/2−)
		2746.8(3)	2					2747(4)	3/2+, 5/2+
		2756.7(3)	2					2757(4)	(3/2+)
	2765.3(3)		(3)					2765.3(6)	(5/2−, 7/2−)
		2766.6(3)	2					2767(4)	(5/2+)
	2812.7(3)		(5)					2812.7(6)	(9/2−, 11/2−)
	2819.5(3)		(3)	2817				2819.5(6)	(5/2−, 7/2−)
		2823.6(3)	4					2824(5)	7/2+, 9/2+
		2831.1(6)	(2)					2831(5)	(3/2+)
	2835.2(3)		(3)	2833				2835.2(6)	(5/2−, 7/2−)
		2844.1(5)	2					2844(5)	3/2+, 5/2+
	2853.7(3)		(3)	2852				2853.7(6)	(5/2−, 7/2−)
		2855.7(3)	2			2891		2856(5)	5/2+
	2859.5(3)		(3)					2859.5(6)	(5/2−, 7/2−)
	2871.2(3)		(3)					2871.2(6)	(5/2−)
	2889.8(3)		(3)					2889.8(6)	(5/2−, 7/2−)
	2899.9(3)		5					2899.9(6)	9/2−, 11/2−
	2919.6(3)		3	2917				2919.6(6)	(5/2−)
	2971.3(3)		3					2971.3(6)	7/2−
	2979.4(3)		3	2975				2979.4(6)	5/2−
				...[g]					
3355.48(19)	3355.6(3)		1					3355.48(19)	3/2−
3429.8(3)	3428.9(3)		1					3429.8(3)	3/2−
	3489.6(3)		1					3489.6(6)	1/2−
3502.59(7)	3503.4(3)		(1)	3498	1			3502.59(7)	(3/2−)
3528.30(14)	3527.7(3)		(1)					3528.30(14)	(3/2−)
3546.92(9)	3545.8(3)		(1)					3546.92(9)	(3/2−)
3564.51(16)	3565.0(3)		1	3560	1			3564.51(16)	1/2−
	3600.5(3)		1					3600.5(6)	(3/2−)
3638.38(6)	3638.4(3)		1					3638.38(6)	1/2−
3648.77(11)	3649.0(3)		1					3648.77(11)	1/2−
	3671.5(3)		1					3671.5(6)	3/2−
	3703.7(3)		1					3707.7(6)	1/2−
	3744.9(3)		1					3744.9(6)	3/2−
	3765.0(3)		1					3765.0(6)	(3/2−)
3792.41(4)	3792.6(3)		1	3788	1			3792.41(4)	3/2−
3852.72(12)	3851.9(3)		1					3852.72(12)	3/2−
3865.37(10)	3865.7(3)		1					3865.37(10)	3/2−
	3899.3(3)		1					3899.3(6)	3/2−
	3948.1(3)		(1)					3948.1(6)	(3/2−)

Table 6 (*continued*)

This work				Other works				Adopted levels	
Level energy E_x (keV)[a]			l	(d, p)[b]		(p, d)[c]	(d, t)[d]		
(n, $\gamma\gamma$)	(d, p)	(d, t)		E_x	l	E_x	E_x	E_x (keV)[e]	J^π
	3969.4(3)		(1)					3969.4(6)	(3/2−)
	3974.3(3)		1					3974.3(6)	3/2−
4032.6(3)	4032.5(3)		1					4032.6(3)	3/2−
	4059.1(3)		1					4059.1(6)	(1/2−)
	4067.8(3)		1	4063	1			4067.8(6)	3/2−
	4082.2(3)		1					4082.2(6)	3/2−
4087.57(12)	4086.8(3)		1	4080	1			4087.57(12)	3/2−
4121.20(9)	4122.1(3)		1					4121.20(9)	1/2−
4133.52(9)	4132.8(3)		1	4121	1			4133.52(9)	3/2−
4175.2(3)	4175.1(3)		1	4167	1			4175.2(3)	(1/2−)
4180.7(3)	4181.2(3)		1					4180.7(3)	(3/2−)
4204.2(3)	4205.9(3)		1					4204.2(3)	1/2−
4220.59(22)	4220.1(3)		1					4220.59(22)	3/2−
4240.5(3)	4239.8(3)		1					4240.5(3)	3/2−
	4267.4(3)		1					4267.4(6)	(1/2−)
4277.03(11)	4277.4(3)		1					4277.03(11)	3/2−
4297.82(21)	4298.5(3)		1					4297.82(21)	1/2−
	4311.7(3)		1					4311.7(6)	(1/2−)
	4336.2(3)		1					4336.2(6)	(1/2−)
4356.15(13)	4356.3(3)		1					4356.15(13)	(1/2−)
4364.58(5)	4365.3(3)		1	4352	(2)			4364.58(5)	1/2−
4374.0(3)								4374.0(3)	(1/2−, 3/2−)
4388.95(10)	4389.1(3)		1	4382	1			4388.95(10)	1/2−
	4425.1(3)		1					4425.1(6)	(3/2−)
4432.94(10)	4433.1(3)		1	4426	1			4432.94(10)	3/2−
	4467.4(3)		(1)	4457	(1)			4467.4(6)	(1/2−)
4588.50(12)				...[h]				4588.50(12)	(1/2−, 3/2−)
6082.42(3)								6082.42(3)	1/2+

[a] The level energies from (n, $\gamma\gamma$) are those of Table 5. The level energies from (d, p) and (d, t) are partly given more accurately in Table 4.

[b] Level energies in keV from Ref. [19].

[c] Level energies in keV, if associated, from Ref. [18] (assignment 2891 keV questionable).

[d] Level energies in MeV, if associated, from Ref. [20].

[e] If the level is only known from (d, p) and/or (d, t), then 0.5 keV systematic error has been added quadratically. Otherwise, the level energies from (n, $\gamma\gamma$) are given. At levels only seen in (d, t) an increasing systematic error above 2 MeV reflects the uncertainty in the energy calibration.

[f] Probably tail of the 180 keV line (250 keV) and background of ^{128}Te(d, t)^{127}Te (see Fig. 6 in Section 2.5).

[g] From here on only levels from (d, p) with $l = 1$ or $l = (1)$ and levels from (n, $\gamma\gamma$) are listed. The missing levels can be seen in Table 4. To the error given there 0.5 keV systematic error has to be added.

[h] Above 4467 keV levels from (d, p) are not listed here, but in Table 4. To the error given there 0.5 keV systematic error has to be added.

particular, all levels below 1 MeV that have been known from β^- decay could be confirmed by the $(n, \gamma\gamma)$ measurement.

Up to 4.5 MeV excitation energy the comparison with earlier neutron stripping reactions shows in general very good agreement. The ^{128}Te(t, d)^{129}Te measurement of Shahabuddin et al. [21], which reached up to 2.5 MeV excitation energy, assignes other l values than we observed only to 5 out of 31 levels. These are the levels 878 keV, 1654 keV, 1753 keV, 2132 keV and 2491 keV (energies from Ref. [21]), where our angular distributions show clearly different values. Furthermore, we saw in (d, p) 12 levels below 2.5 MeV which remained obscured for Shahabuddin et al. because of their energy resolution of 15 keV. A comparison with the relatively old measurement of Moore et al. [19] shows very good agreement up to 4.5 MeV excitation energy. The energy deviations to the present (d, p) and $(n, \gamma\gamma)$ measurements are in the most cases less than 5 keV, as can be seen from Table 6. However, we observed much more levels especially between 3 MeV and 4.5 MeV. This is very useful concerning the comparison with the $(n, \gamma\gamma)$ measurement with respect to the so-called direct neutron capture, as will be seen later. Just in this energy region altogether 26 levels with $l = 1$ have been observed also in $(n, \gamma\gamma)$. The only discrepancy between the earlier and the present neutron stripping reactions is the behaviour of the spectroscopic factors. Although the spectroscopic factors have been adjusted to the old measurements (cp. Section 2.7) they become clearly smaller in our measurement especially for levels with $l = 1$ above 1 MeV.

The comparison with earlier neutron pickup reactions is difficult because of the deviating energy calibrations of the (p, d) measurement of Galès et al. [18] and the (d, t) measurement of Jolly [20].

In Table 6 the levels observed earlier have been associated as far as possible with those of our $(\vec{d}, t)$ measurement. As can be seen, the old measurements disagree already at 1.3 MeV by 20 keV.

The $(\vec{d}, t)$ measurement was a helpful tool for the determination of unambiguous J^π assignments as showed already Table 4. In the region below 3 MeV excitation energy 71 levels could be observed instead of earlier 28 levels [18].

Altogether, the situation in the level scheme of ^{129}Te has become much clearer already below 1.5 MeV excitation energy. We observed in this region 21 levels with unambiguous J^π assignment (with two exceptions). In contrast, in the Nuclear Data Sheets [22] 27 levels are listed with a J^π being unambiguous only in seven cases, while the existence of some levels was questionable.

4. Thermal neutron capture cross section of ^{128}Te

Besides the value of the thermal neutron cross section of ^{128}Te recommended in the BNL neutron cross section atlas [41], $\sigma_{n\gamma}^{g+m} = 215$ mb, other values were reported in the range from 148 mb to 216 mb [42–44].

To calculate new values for the thermal neutron capture cross section we used the intensities of three strong γ lines (see Table 1) and the partial elemental cross sections

Table 7
Determination of the thermal neutron capture cross section of ^{128}Te

E_γ (keV)	I_γ (%)	$\sigma_{n\gamma}^{elem}$ (mb) [45]	$\sigma_{n\gamma}$ (mb)
359.2	7.6(8)	4.5(7)	187(35)
3377.3	10.4(10)	5.5(9)	167(32)
3702.8	10.3(10)	7.1(12)	218(43)
	Mean value		186(21)

$\sigma_{n\gamma}^{elem}$ from a preliminary measurement at Budapest with a natural Te target [45]. The thermal neutron capture cross section can be calculated via

$$\sigma_{n\gamma} = \frac{\sigma_{n\gamma}^{elem}}{Ab^{128} \times I_\gamma}, \tag{2}$$

with Ab^{128} being the abundance of ^{128}Te in the element (31.69%). The results of this calculation are given in Table 7.

The weighted average value is $\sigma_{n\gamma}^{g+m} = 186 \pm 21$ mb. With our new information about the decay scheme of ^{129}Te we can also calculate new separate values for the (n, γ) cross sections for the formation of ^{129g}Te and ^{129m}Te, the ground state and the metastable state, respectively. The sum of the intensity feeding the ground state is 82.3%, to which the contribution of inner conversion of the strong 180 keV γ line (10% of 44%) has to be added, giving 86.7%. The summed intensity feeding the $11/2^-$ isomer is 10.7%, and with the amount of inner conversion of the 359 keV γ line (2% of 7.6%) the sum is 10.85%. (The conversion coefficients have been taken from Ref. [24].) This means, the ratio between the cross sections for the formation of the ground state and the formation of the metastable state is $86.7/10.85 = 8$. This results in new values for $\sigma_{n\gamma}^{129g} = 165(20)$ mb and $\sigma_{n\gamma}^{129m} = 21(3)$ mb that are quite different from the values given in Ref. [41] ($\sigma_{n\gamma}^{129g} = 200(8)$ mb and $\sigma_{n\gamma}^{129m} = 15(1)$ mb).

The sum of the intensity feeding the ground state and the intensity feeding the isomer of 97.55% reflects the approached completeness of the level scheme.

5. Comparison with theoretical models

As a result of the light particle transfer reaction and the (n, γ) reaction studies we have now a rather detailed knowledge of the low spin states in the first few MeV of excitation of this nucleus. We shall attempt now to understand these states in terms of two different theoretical models: the interacting boson–fermion model (IBFM) and the quasiparticle phonon model (QPM). Each of these two models takes into account certain degrees of freedom of the nuclear excitations, the difference between them resulting mainly of the philosophy adopted with respect to the truncation of the real many-body problem (the full shell model approach). The comparison of their results with the experimental data, as well as a comparison between the results of the two models will lead to a better understanding of the limits of each of them.

5.1. The interacting boson–fermion model calculations

The IBFM, an extension of the interacting boson model (IBM) [46] to the odd-mass nuclei, is constructed for the description of the low-lying collective states. A first important approximation is that only the nucleons outside closed shells, which may be particles or holes, are considered to be responsible for the lowest excitations. Secondly, in an even–even nucleus, these valence nucleons are replaced by a system of N (N is half of the number of valence nucleons) s- and d-bosons; in the odd-A nuclei, a fermion (the odd nucleon) is coupled to the system of bosons representing the even–even core. These approximations proved to be extremely good for low-lying nuclear excitations, making the IB(F)M a versatile model for most medium and heavy mass nuclei. On the other hand, when comparing the predictions of this model to experimental data which extend a few MeV in excitation energy, one should bear in mind that one of its strong limitations is the assumption of an inert core, which in reality breaks down at 2–3 MeV excitation, where a much richer variety of excitations is observed.

The present calculations are made with the IBFM-1 variant of the model [47], in which no distinction is made between neutrons and protons. This model was employed in a previous work for the description of the evolution of the low-energy spectra in the Te isotopes ^{119}Te to ^{129}Te; the details concerning the Hamiltonian used and the procedure by which the values of the model parameters were chosen, can be found in Ref. [2], and results for different isotopes of this chain in Refs. [1,4,7]. Here we wish to compare the results of these calculations with the present, more detailed spectroscopic information we have now on ^{129}Te.

The ^{129}Te nucleus is described in this model as consisting of a ^{130}Te core to which one couples one fermion (a neutron hole). In the IBM description, this core has three bosons: one proton boson, and two neutron (hole type) bosons. The lowest excitations of the core could be reasonably described by an IBM Hamiltonian which is very close to the U(5) dynamical symmetry limit (anharmonic vibrator). One should remark, however, that around 2 MeV excitation there are states in the core nucleus which cannot be accounted for by this description [2]; also, in this description we do not consider the octupole degrees of freedom, which are present at about 2 MeV.

The odd fermion was allowed to occupy the valence shell model orbitals (from the 50–82 major shell) $2d_{5/2}$, $1g_{7/2}$, $2d_{3/2}$, $3s_{1/2}$ and $1h_{11/2}$; due to limitations of the ODDA code [48,49], either the orbitals $2f_{7/2}$, $1h_{9/2}$, $3p_{3/2}$, $3p_{1/2}$ or $1f_{7/2}$, $1f_{5/2}$, $2p_{3/2}$, $2p_{1/2}$, have been considered in separate calculations, in addition to the negative parity orbital $1h_{11/2}$, in order to get an estimation of the fragmentation of the low-spin negative parity orbitals in the neutron stripping and pickup, respectively. What is remarkable in these calculations is that for both parities and all isotopes with mass 119 to 129 the boson–fermion interaction strength parameters could be kept constant ($\Gamma_0 = 0.2$ MeV and $\Lambda_0 = 0.95$ MeV^2 for the quadrupole and exchange interaction, respectively). A detailed comparison with the present ^{129}Te data is given in the following.

5.1.1. Positive parity states

Fig. 9 shows a comparison of the experimental spectrum of states of positive parity with the calculated one. The lowest states up to about 1.5 MeV excitation can be readily associated with calculated ones, as shown in the figure. This correspondence is made on

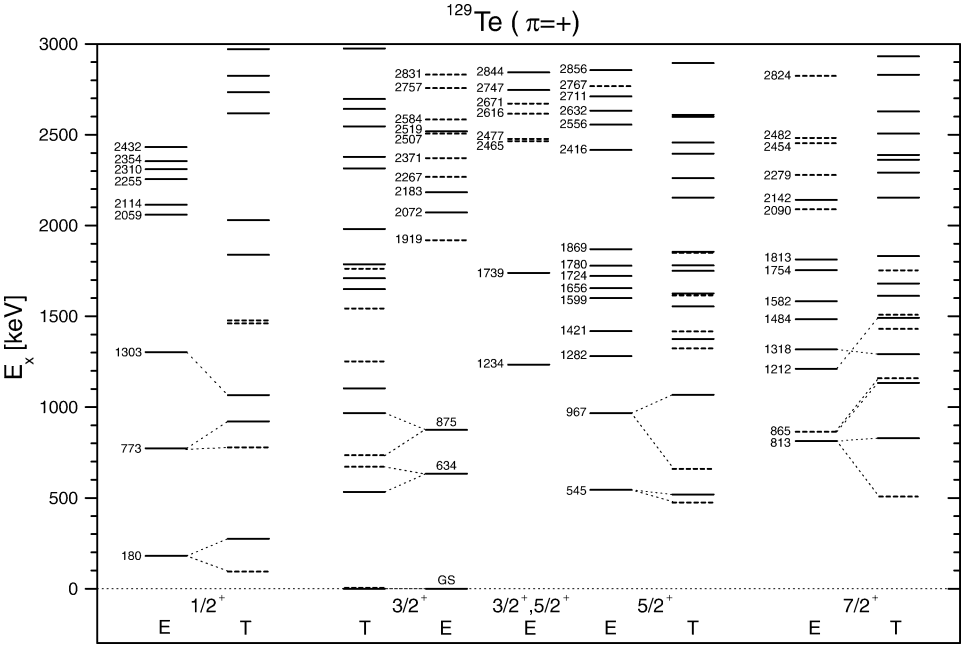

Fig. 9. Comparison between the experimental (E) and calculated (T) positive parity levels of ^{129}Te. All experimental and IBFM levels below 3.0 MeV are shown. Solid lines for the theory values represent results of the IBFM, dashed lines of the QPM. QPM levels are shown here only up to 2 MeV. For all levels compare Fig. 12. Dashed experimental levels refer to unsafe assignments. The indicated correspondences between experimental and calculated levels are based on the level positions and their electromagnetic decay properties. Numbers are excitation energies in keV.

the basis of the excitation energy, as well as of the electromagnetic decay properties (which consist mainly of branching ratios) and spectroscopic factors for neutron transfer. The experimental and predicted branching ratios for the lowest states are compared in Table 8 in Section 5.3; in general, the branching ratios are correctly described. Other decay properties like, for example, absolute transition probabilities and E2/M1 mixing ratios are not known experimentally. For the $3/2^+$ ground state the known static moments [22] $\mu = 0.702(4)$ nm and $Q = 0.055(13)$ b are reasonably well predicted as $\mu = 0.801$ nm and $Q = 0.095$ b, respectively.

The structure of the wavefunctions of the lowest four positive parity states of low spins is shown in Fig. 10. While the first state of each spin from $1/2$ to $7/2$ is an almost pure quasiparticle state, dominated by the $s_{1/2}$ or $d_{3/2}$ orbital, the higher states contain various admixtures between the four orbitals, $s_{1/2}$ and $d_{3/2}$ still dominating in most of them. The experimental and the calculated one-neutron transfer spectroscopic strength is shown in Fig. 11. The predicted values can be easily correlated with the structure of the wavefunctions, as shown in Fig. 10. Against the predictions of the IBFM, above 1.5 MeV excitation levels are hardly seen both in the (d, p) and the (d, t) experiment. This is probably due to the strong influence of non-statistical effects in ^{129}Te that will be reviewed later.

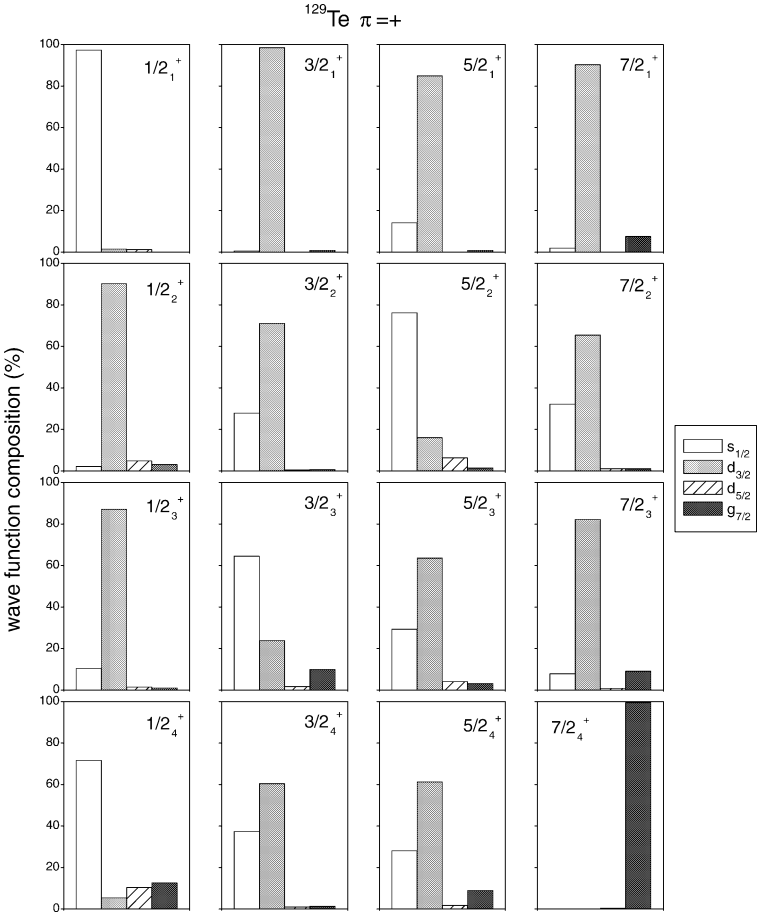

Fig. 10. The composition of the IBFM wavefunctions for the lowest levels of positive parity in ^{129}Te.

Above 1.5 MeV excitation it becomes difficult to make a one-to-one correspondence between the experimental and theoretical levels, because the experimental data are not completely unambiguous. The number and general pattern of the calculated levels resembles well those of the experimental scheme up to about 2.2 MeV. On the other hand, this might be a region where boson cut-off effects already start to play a role. Indeed, anticipating a bit the discussion about the second model employed in this work, Fig. 12 shows a comparison of the level schemes calculated with the IBFM and QPM, respectively. It is evident that in the IBFM case the level density starts being smaller already above 2 MeV, which suggests the importance of other excitation modes at higher energies.

5.1.2. Negative parity states

The comparison between the experimental and calculated spectra of levels with negative parity is given in Fig. 13. The lowest state of each spin between $1/2$ and $11/2$, as well as the second $3/2$ and $7/2$ states are in good agreement with the observations. All these states

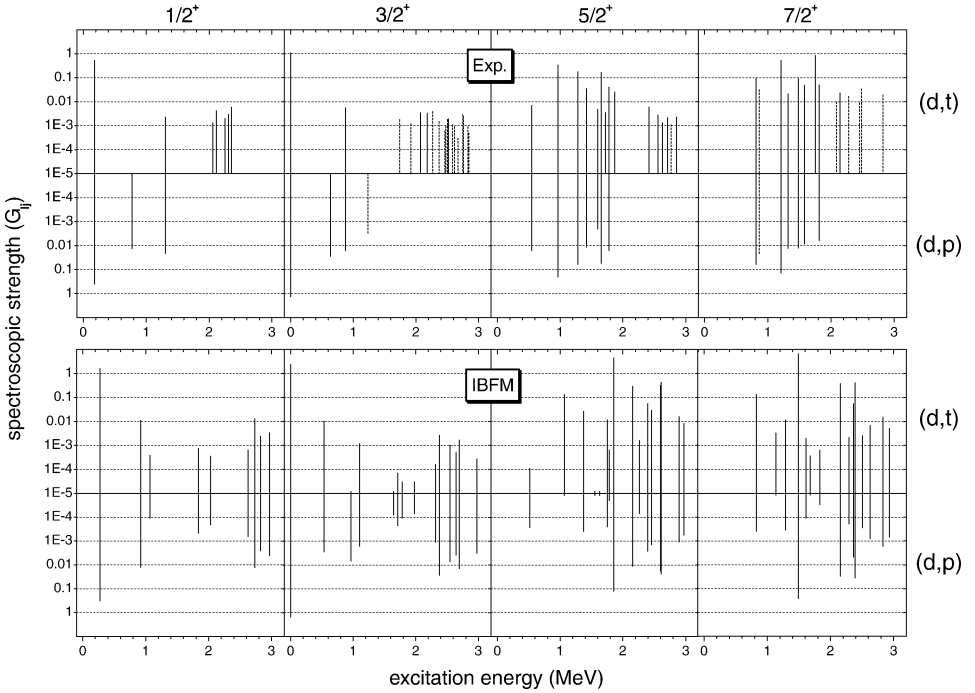

Fig. 11. Experimental and calculated (IBFM) spectroscopic factors for one-neutron pickup and stripping, respectively, for the low spin states of positive parity. Very small theoretical values of 1.5×10^{-5} are drawn to show the existence of some levels, even if the calculated strength is smaller.

belong to the $h_{11/2}$ family (i.e., their structure is largely dominated by the $h_{11/2}$ orbital coupled to states of the core). The correspondences shown in Fig. 13 are also made on the basis of the γ-decay branchings, which are well described by the calculations (see Table 8 in Section 5.3).

An exception is the first $1/2$ state: The calculated state, which is the highest anti-aligned state (i.e., it results from the antiparallel coupling of the $h_{11/2}$ quasiparticle to the highest spin state of the $N = 3$ boson core ($J = 6$)) could not be clearly correlated to an experimental level, especially because the lowest experimental levels assigned as $(1/2)$ from (d, p) have not been seen in the (n, γ) measurement.

For the higher excited states it is difficult to see how far the agreement with the calculations goes. The number of observed states with low spin (like $3/2$) is much larger than the number of calculated IBFM states in the same energy region. This can probably be related to the boson cut-off effect and consequently the IBFM becomes unrealistic at energies above 2 MeV, as it can be seen in the direct comparison with the results of the QPM in Fig. 12. Only the QPM model reproduces correctly the rising level density.

5.2. The quasiparticle–phonon model calculations

The quasiparticle–phonon model (QPM) was suggested in late seventies by Soloviev [50]. The excited states in even–even nuclei are described in this model as phonons

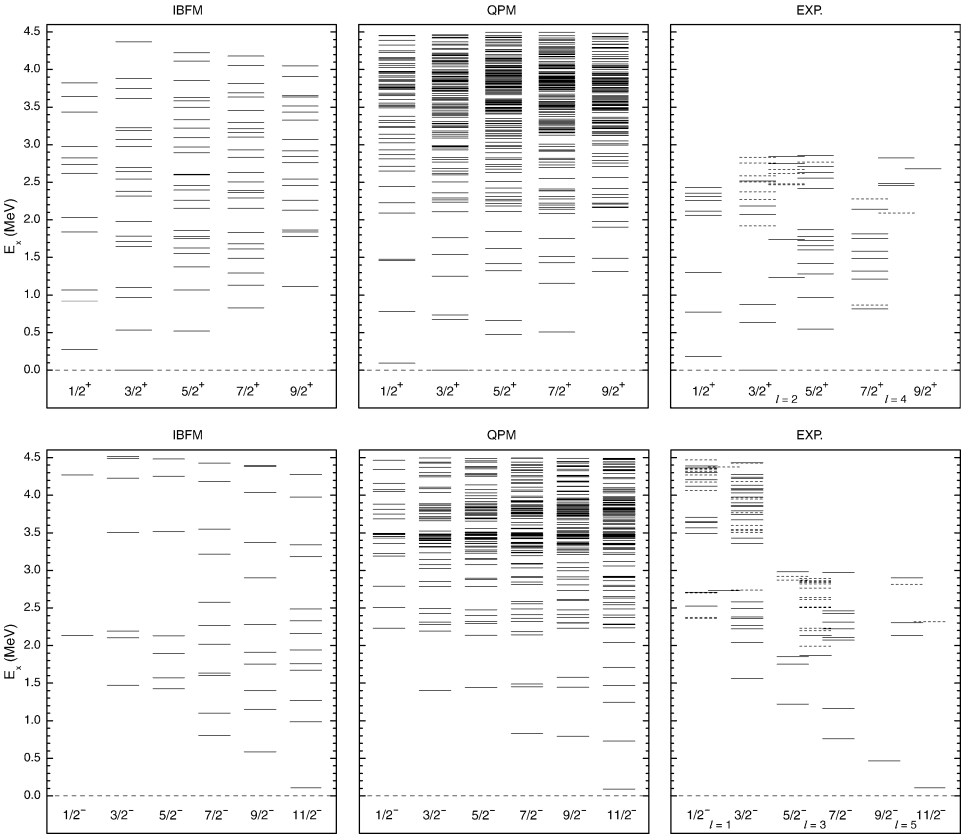

Fig. 12. Comparison between the level schemes calculated with the IBFM and the QPM, and the experimental level scheme. The experimental level scheme shows all levels of Table 6. Dashed lines refer to unsafe assignments.

which are solutions of quasiparticle-RPA equations and include both collective and non-collective particle–hole modes. Complex configurations are treated as multi-phonon states by coupling of phonons of different multipolarity and parity. A realistic interaction of the nucleons is replaced by an effective interaction in a separable form. Strength parameters of the interaction are fitted to experimental data for correct description of the lowest collective states. In odd nuclei, phonons are coupled to an extra unpaired quasiparticle on different levels of a mean field. General ideas of the QPM and its formalism to describe excited states in spherical nuclei with odd mass number are given in Ref. [51]. A detailed description of our QPM calculations to ^{131}Te is given in Refs. [10,14]. They are analog to the calculations to ^{129}Te presented here.

Fig. 14 shows a comparison between the experimental (d, p) spectroscopic factors and the results of our calculations for the first excited states. The QPM model reproduces reasonably well the spectroscopic factors, in many cases better than the IBFM calculations.

The correspondences between calculated and experimental states have been made also via the branching ratios, given in Table 8 (Section 5.3). The deviations in energy between

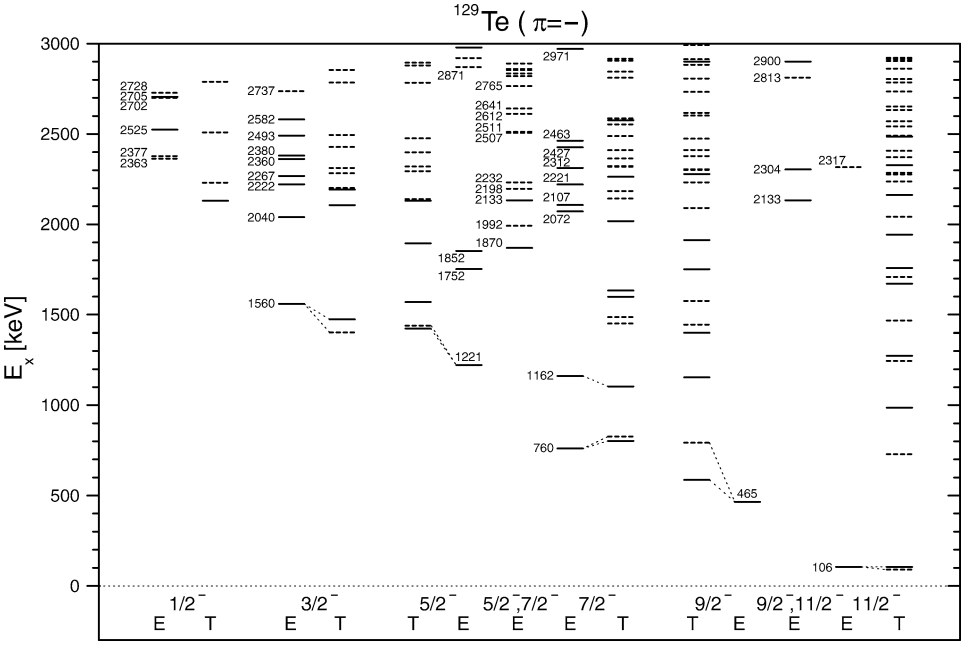

Fig. 13. Comparison between the experimental (E) and calculated (T) negative parity levels of ^{129}Te. All levels below 3.0 MeV are shown. Solid lines for the theory values represent results of the IBFM, dashed lines of the QPM. Dashed experimental levels refer to unsafe assignments. Numbers are excitation energies in keV.

calculated and experimental low lying states are comparable to the results of the IBFM, as could already be seen in Figs. 9 and 13. However, the comparison of the level densities shows that the QPM is able to describe the increasing level density above 2 MeV excitation energy much better than the IBFM (see Fig. 12).

Fig. 15 gives an impression of the experimental and calculated distributions of $3p_{1/2}$ and $3p_{3/2}$ strengths up to 5.5 MeV and 5 MeV, respectively. This comparison is possible because of the detailed experimental information on $1/2^-$ and $3/2^-$ states at high excitation energies. One observes a lack of calculated $1/2^-$ states with relatively large cross sections below 4.8 MeV, while the fragmentation of the $3p_{3/2}$ strength seems to be better reproduced. The same situation is observed in ^{131}Te. For a more detailed discussion see Ref. [14].

5.3. Branching ratios

The experimental and predicted branching ratios for the lowest states are compared in Table 8; in general, the branching ratios are correctly described by the calculations within the both models.

The IBFM calculations of electromagnetic transition probabilities are described in detail in Ref. [2]. Since we have used a large mean field basis in the QPM, no effective charges are needed for the calculation of the E2 transition matrix elements within this model, i.e., $e^{(\mathrm{E2})}(n) = 0$ and $e^{(\mathrm{E2})}(z) = 1$. For the M1 transition operator we have used $g_s^{\mathrm{eff}} = 0.8\, g_s^{\mathrm{free}}$

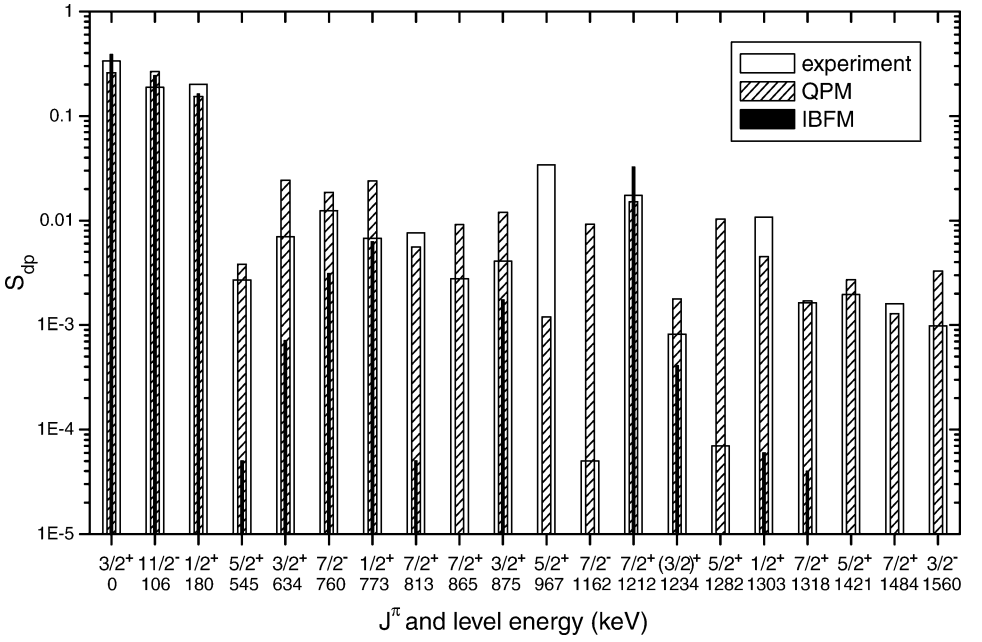

Fig. 14. Comparison between the experimental (d, p) spectroscopic factors and the IBFM and QPM predictions for low lying states of ^{129}Te. The states are ordered by rising experimental energy (cp. Table 6). For this figure a $3/2^+$ assignment was assumed for the 1234 keV state. Some correlations are tentative and they are not shown in Figs. 9 and 13.

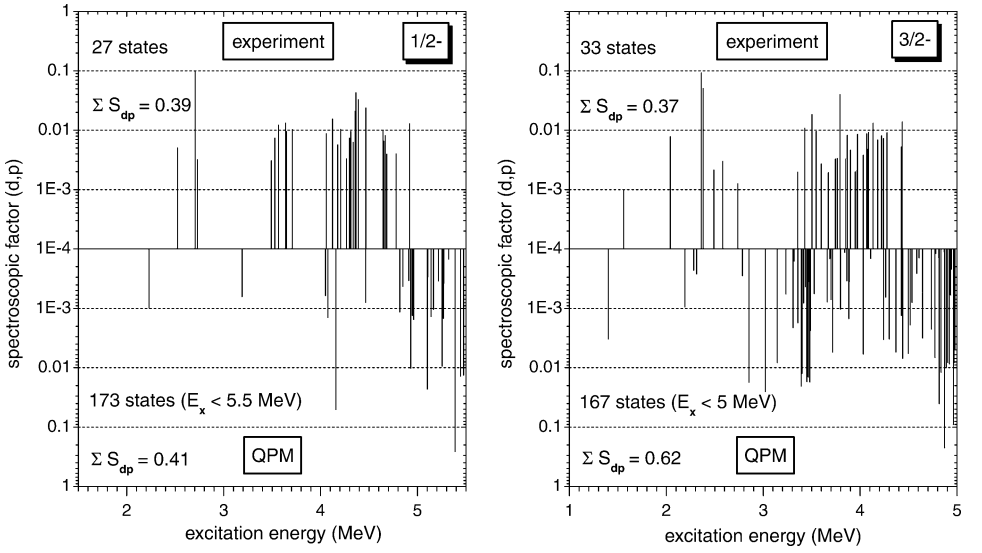

Fig. 15. Comparison between the experimental (d, p) spectroscopic factors and the QPM calculation predictions for $3p_{1/2}$ and $3p_{3/2}$.

Table 8
Experimental and theoretical electromagnetic properties of low-lying ^{129}Te states. The theoretical branching ratios are calculated with experimental level energies. B(E2) and B(M1) are the reduced transition probabilities

				Exp.	IBFM			QPM		
E_x (MeV)	J_i^π	J_f^π	E_γ (MeV)	$Br.$ (%)	$Br.$ (%)	B(E2) (e^2b^2)	B(M1) (μ_{N^2})	$Br.$ (%)	B(E2) (e^2b^2)	B(M1) (μ_{N^2})
0.180	$1/2_1^+$	$3/2_1^+$	0.180	100	100	2.3×10^{-2}	1.7×10^{-8}	100	1.2×10^{-4}	0.0
0.465	$9/2_1^-$	$11/2_1^-$	0.359	100	100	4.4×10^{-2}	3.6×10^{-3}	100	4.5×10^{-2}	1.0×10^{-4}
0.545	$5/2_1^+$	$3/2_1^+$	0.545	100	100	4.1×10^{-2}	3.5×10^{-4}	100	1.4×10^{-2}	6.8×10^{-2}
		$1/2_1^+$	0.364	2.8	2.4	7.4×10^{-3}	0.0	0.3	9.6×10^{-3}	0.0
0.634	$3/2_2^+$	$3/2_1^+$	0.634	100	100	3.9×10^{-2}	2.6×10^{-4}	100	2.4×10^{-2}	2.6×10^{-1}
		$1/2_1^+$	0.453	25.8	6.7	1.4×10^{-2}	2.6×10^{-5}	0.7	8.4×10^{-4}	0.0
		$5/2_1^+$	0.089	–	4.2	6.8×10^{-3}	1.7×10^{-1}	0.9	1.0×10^{-2}	8.8×10^{-1}
0.760	$7/2_1^-$	$11/2_1^-$	0.654	100	100	3.8×10^{-2}	0.0	100	3.8×10^{-2}	0.0
		$9/2_1^-$	0.295	43.2	74.8	2.4×10^{-5}	9.4×10^{-2}	<0.1		
0.773	$1/2_2^+$	$3/2_1^+$	0.773	100	100	3.4×10^{-2}	8.2×10^{-4}	100	4.2×10^{-2}	0.0
		$1/2_1^+$	0.593	31.9	12.2	0.0	4.1×10^{-3}	4.9	0.0	1.9×10^{-1}
		$3/2_2^+$	0.139	–	3.0	7.0×10^{-3}	7.8×10^{-2}	<0.1		
0.813	$7/2_1^+$	$3/2_1^+$	0.813	100	100	5.0×10^{-2}	0.0	100	3.4×10^{-2}	0.0
		$5/2_1^+$	0.268	–	4.0	1.8×10^{-2}	2.5×10^{-2}	<0.1		
0.865	$7/2_2^+$	$5/2_1^+$	0.321		100	9.0×10^{-3}	4.1×10^{-3}	14.5	3.7×10^{-3}	0.0
		$3/2_1^+$	0.865		70.7	3.3×10^{-4}	0.0	100	1.7×10^{-4}	0.0
		$3/2_2^+$	0.231		13.0	4.4×10^{-2}	0.0	0.2	7.3×10^{-4}	0.0
0.875	$3/2_3^+$	$3/2_1^+$	0.875	100	100	1.1×10^{-2}	9.0×10^{-4}	17.5	2.6×10^{-3}	1.4×10^{-2}
		$1/2_1^+$	0.694	68.2	76.0	2.9×10^{-2}	6.8×10^{-6}	100	4.8×10^{-2}	0.0
		$5/2_1^+$	0.330	34.6	42.2	1.6×10^{-4}	5.1×10^{-2}	0.5	3.8×10^{-3}	4.4×10^{-2}
		$3/2_2^+$	0.241	–	18.7	2.3×10^{-4}	5.8×10^{-2}	0.1	9.6×10^{-3}	2.3×10^{-2}
0.967	$5/2_2^+$	$3/2_1^+$	0.967	100	100	5.9×10^{-3}	3.1×10^{-2}	100	1.7×10^{-2}	2.0×10^{-2}
		$1/2_1^+$	0.786	33.6[a]	28.5	4.3×10^{-2}	0.0	17.8	8.3×10^{-3}	0.0
		$5/2_1^+$	0.422	–	43.2	6.0×10^{-3}	1.8×10^{-1}	0.2	2.5×10^{-5}	2.3×10^{-2}
		$3/2_2^+$	0.333	–	22.7	2.4×10^{-2}	1.9×10^{-1}	0.1	1.8×10^{-3}	2.3×10^{-2}
		$3/2_3^+$	0.092	–	0.9	1.6×10^{-4}	3.7×10^{-1}	<0.1		
1.162	$7/2_2^-$	$9/2_1^-$	0.698	100	100	4.7×10^{-2}	2.9×10^{-2}	100	2.0×10^{-2}	0.0
		$7/2_1^-$	0.402	–	2.8	4.0×10^{-3}	6.0×10^{-3}	2.8	8.8×10^{-3}	1.6×10^{-3}
		$11/2_1^-$	1.057	7.9	0.2	2.9×10^{-5}	0.0	<0.1		
1.221	$5/2_1^-$	$9/2_1^-$	0.757	100	100	1.4×10^{-2}	0.0	100	2.8×10^{-3}	0.0
		$7/2_1^-$	0.461	21.1	32.9	3.8×10^{-2}	2.5×10^{-3}	79.8	2.6×10^{-2}	1.7×10^{-2}
		$7/2_2^-$	0.059	–	1.9	7.2×10^{-4}	2.2×10^{-1}	<0.1		
1.560	$3/2_1^-$	$5/2_1^-$	0.339	71.4	100	1.3×10^{-4}	3.9×10^{-1}	<0.1		
		$7/2_1^-$	0.800	100	78.7	5.2×10^{-2}	0.0	100	3.4×10^{-2}	0.0

[a] Multiply placed, undivided intensity given (see Table 1). The placement of this γ transition is not confirmed by coincidences.

and $g_l(n) = 0$ and $g_l(z) = 1$. The main components of the wavefunctions of the low-lying states in Table 8 are quasiparticle configurations (qp_j) and configurations of quasiparticles coupled to the lowest collective 2_1^+ phonon ($[qp_{\tilde{j}} \otimes 2_1^+]_j$). Thus, the M1 decays presented in Table 8 are due to $qp_j \to qp_{j'}$ and $[qp_{\tilde{j}} \otimes 2_1^+]_j \to [qp_{\tilde{j}'} \otimes 2_1^+]_{j'}$ transitions. Since ^{129}Te is an odd-n nucleus and $e^{(2)}(n) = 0$, such transitions do not contribute to the E2 decays. The latter are determined by an exchange of the phonon $[qp_{\tilde{j}} \otimes 2_1^+]_j \to qp_{\tilde{j}}$ and $qp_{\tilde{j}} \to [qp_{\tilde{j}} \otimes 2_1^+]_j$.

6. Direct capture in the ^{128}Te(n, γ)^{129}Te reaction

It is known since a long time that nuclei with mass numbers in the region of 40 and 140 show intensities of γ radiation following thermal neutron capture with regularities that are not in agreement with the statistical theory of the decay of higly excited states. This behaviour expresses itself in a strong correlation between primary (n, γ) intensities and spectroscopic factors of (d, p). Lane and Lynn developed a theory of so-called direct neutron capture which describes this correlation [52].

Mughabghab was able to show good agreement between theoretical (calculated from (d, p) spectroscopic factors according to the Lane–Lynn theory) and experimental (n, γ) cross sections [53].

Also in the ^{128}Te(n, γ)^{129}Te reaction the direct neutron capture plays an important role as shown by Honzátko et al. already in 1981 [17]. ^{128}Te lies in the favoured mass region of the direct capture of thermal neutrons and its capture cross section is so small (0.215 b [41] and see Section 4) that the direct capture can be observed without being obscured because of statistical compound-nucleus processes.

Within the new study of the odd tellurium isotopes our group has proven direct capture also at the target nuclei ^{126}Te [54] and ^{130}Te [13]. The results of the ^{128}Te(n, γ)^{129}Te experiment reported in this paper are shown in Fig. 16.

In the upper part the x-axis is the partial (n, γ) cross section $\sigma_{\gamma f} = I_{\gamma f}\sigma_\gamma$, where $I_{\gamma f}$ is the intensity of a primary γ line feeding a level seen with $l = 1$ in (d, p) (cp. last page of Table 5). The point with the largest cross section, for example, belongs to the γ line 3722 keV with $\sigma_{\gamma f} = 42$ mbarn.

The y-value is the theoretical capture cross section σ_{DC} calculated according to the Lane–Lynn theory. The formula is given in Ref. [41], p. 12. This value is directly proportional to the spectroscopic strength $(2J+1)S_{lj}$ of that level in (d, p) that is populated by the corresponding primary γ transition (cp. Table 4). So the level with $l = 1$ at 6082 keV − 3722 keV = 2360 keV has the largest spectroscopic strength, for example. The dashed line in Fig. 16 shows the linear dependency of both cross sections. A straight line with slope one, where the points should lie in the ideal case, is also shown. The deviation has its reason in too small (d, p) spectroscopic factors (about a factor of two). Like already mentioned in Section 2.7 the spectroscopic factors have been fitted to the values of Moore et al. [19] for the first three levels. Nevertheless we get values for the higher states with $l = 1$, which lie about 50% below the values of Ref. [19]. This might be related to the fact that Moore et al. stayed with $E_d = 7.5$ MeV remarkably under the Coulomb

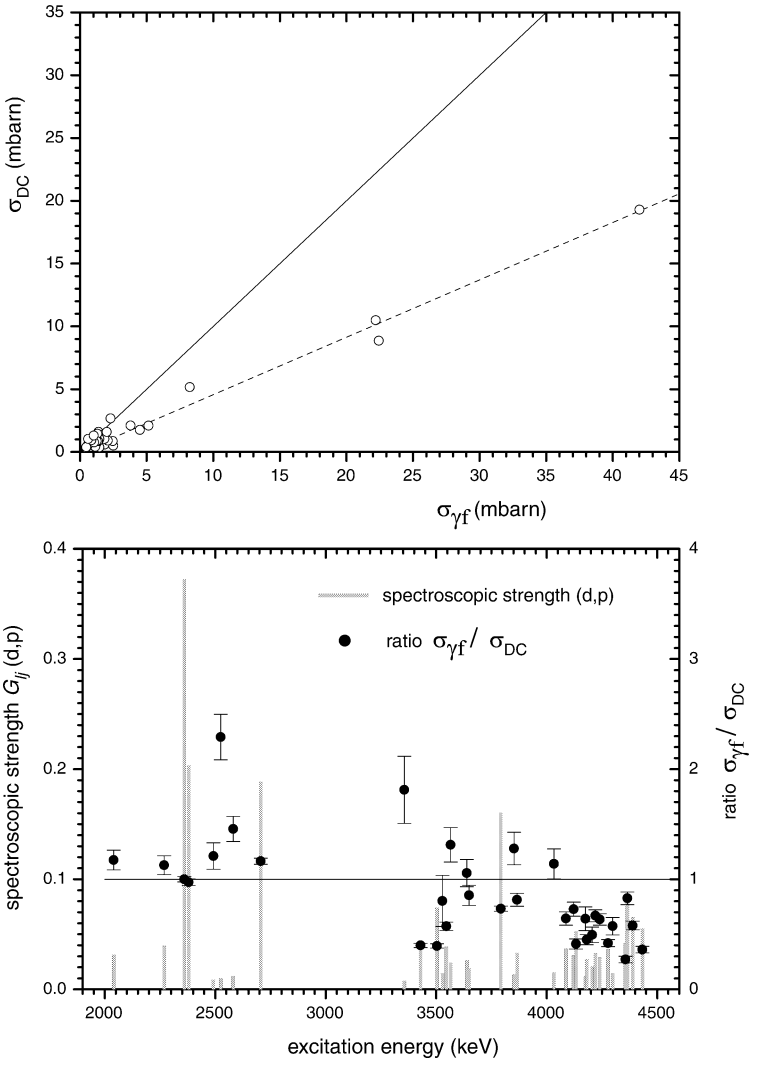

Fig. 16. Direct capture in ^{128}Te. Upper part: Cross sections from the Lane–Lynn theory and from (n, γ). The dashed line is a linear fit to the points. Lower part: (d, p) spectroscopic strength (grey lines and left scale) and ratio of the (n, γ) cross sections to σ_{DC} of the Lane–Lynn theory (dots and right scale) over the excitation energy. The ratio is normalized to one for the strongest line (2360 keV).

barrier of approx. 11.5 MeV, which resulted in poorly structured angular distributions. In the publication of Honzátko et al. [17] where the results of the (d, p) measurement of Moore et al. have been used, a very good one-to-one agreement between σ_{DC} and $\sigma_{\gamma\mathrm{f}}$ has been reached through an adjustment of the coherent scattering length (which was not well known so far) in the Lane–Lynn formula. The adopted value was $a_{\mathrm{coh}} = 5.2$ fm, while a new measurement of Koester et al. [55] obtained a value $a_{\mathrm{coh}}(^{128}\mathrm{Te})$ of 5.88(7) fm.

However, also with the new experimental data the importance of the direct neutron capture in the ^{128}Te(n, γ)^{129}Te reaction is obvious. The lower part of Fig. 16 shows another illustration. With the help of the excitation energy every level can be identified. Fig. 16 shows that at higher excitation the cross section ratio becomes systematically lower.

7. Isomer population

A particularly strong population of the long-lived $h_{11/2}$ isomer of the odd tellurium isotopes has been observed in various reactions. The detailed study of the level scheme of ^{129}Te could reveal the mechanism which is responsible for this strong population. A clue for the understanding is the newly established $5/2^-$ level at 1221 keV [56]. This level picks up effectively intensity from higher lying $3/2^-$ states, which are primarily fed through direct neutron capture, and which also have strong branchings to the ground state. Approximately 42% of the intensity that feeds the isomer go through this level. Besides that the newly found $7/2^-$ state at 1162 keV plays an important role with about 25% participation. Except for the $7/2^-$ state all low lying states of negative parity are only weakly populated in (d, p). This is a sign for their complicated structure as mentioned in Refs. [21,38]. The IBFM describes the $3/2^-$ and $5/2^-$ states as a mixture of the $1h_{11/2}$ neutron wavefunction as a main part with a small $3p$ component, coupled to the first 4^+ state of the core [56,57]. The IBFM calculations reproduce well the energy of the states (see Fig. 13) and confirm the enhanced E2 transitions between the levels of negative parity due to the admixed quadrupole phonons. Our collaboration has found very similar mechanisms of the isomer population in ^{123}Te, ^{125}Te [56] and ^{131}Te [13,14].

8. Conclusions

The present study is a part of the systematic investigation of the tellurium isotopes by our collaboration. The combination of neutron-pickup and neutron-stripping reactions leads to an elaborate level scheme. The information on quantum numbers of the low lying states was improved drastically and the $\gamma\gamma$ coincidence measurements have produced a detailed decay scheme.

The new experimental results have been compared with the theoretical IBFM and QPM models. Both are able to reproduce quite well the properties of the low lying excited states, while the limits of the IBFM become evident at higher excitation energies.

The interesting non-statistical effects of the strong isomer population and the direct neutron capture have been studied in more detail than the experimental situation allowed before.

Acknowledgements

This work was supported by the DFG under IIC4-Eg 25/4-1 and by the Grant Agency of the Czech Republic (No. 202/99/K038 and No. 202/99D087). We wish to thank P. Maier-Komor, K. Nacke, H.-J. Maier and D. Frischke for the target preparation and T. Faestermann for the Q3D maintenance.

Appendix A. Input files for the DWBA calculations

Fig. 17 shows three examples of CHUCK3 input files for different states in the measured transfer reactions ^{128}Te(d, p)^{129}Te at $E_d = 24$ MeV and $E_d = 18$ MeV, and ^{130}Te($\vec{d}$, t)^{129}Te at $E_d = 24$ MeV. Results of the calculations can be seen in Fig. 3 and Fig. 7.

```
1009000030000000    128TE(D,P)129TE EX=.180 MEV S1/2 ED=24 MEV
+81.    +05.    +0.5
+30+02+00+01
+00.1   +20.
+24.0   +2.0136 +01.    +128.00 +52.    +01.15          +00.54  +02.
+01+01
+01.    -105.93 +1.120  +0.770
+02.                                    +62.71  +1.320  +0.850
-04.    -15.600 +1.1600 +0.8400
+03.859 +01.0078+01.    +129.00 +52.    +01.25          +00.85  +01.    -0.180
+02+02
+01.    -51.96  +1.2200 +0.670
+02.                                    +36.67  +1.230  +00.670
-04.    -30.0   +01.22  +00.67
-02-01+00+01+01+01+00+00+0122.00                         +0.621
-06.083 +01.0087+00.    +128.00 +52.    +01.25          +00.85          +0.180
-01.    -01.    +01.17  +00.75  +25.
+02.    +00.    +01.    +01.    +60.
+00+00
9                           END OF CHUCK3 INPUT


1009000030000000    128TE(D,P)129TE EX=2.360 MEV P3/2 ED=18 MEV
+51.    +05.    +1.0
+30+02+00-03
+00.1   +20.
+18.0   +2.0136 +01.    +128.00 +52.    +01.15          +00.54  +02.
+01+01
+01.    -113.17 +1.120  +0.810
+02.                                    +68.80  +1.320  +0.910
-04.    -15.600 +1.1600 +0.8400
+03.859 +01.0078+01.    +129.00 +52.    +01.25          +00.85  +01.    -2.360
+02+02
+01.    -56.12  +1.2200 +0.77
+02.                                    +56.46  +1.230  +00.770
-04.    -30.0   +01.22  +00.67
-02-01+01+01+03+01+00+00+0122.00                         +0.621
-06.083 +01.0087+00.    +128.00 +52.    +01.25          +00.85          +2.360
-01.    -01.    +01.17  +00.75  +25.
+02.    +01.    +03.    +01.    +60.
+00+00
9                           END OF CHUCK3 INPUT


1009000030000000    130TE(D,T)129TE EX=.105 MEV H11/2
+80.    +05.    +0.5
+30+02+00-11
+00.1   +20.
+24.0   +2.0136 +01.    +130.00 +52.    +01.15          +00.54  +02.
+01+01
+01.    -96.50  +1.1330 +0.7700
+02.                                    +48.00  +01.321 +00.68
-04.    -13.660 +1.0700 +0.6600
-02.154 +03.016 +01.    +129.00 +52.    +01.30          +00.25  +01.    -0.105
+02+02
-01.    -150.24 +1.2400 +0.6870         -20.00  +01.430 +00.87
-02-01+05+01+11+01+00+00-225.00                          -0.845
-08.419 +01.008 +00.    +129.00 +52.                    +00.85          +0.105
-01.    -01.    +01.17  +00.75  +25.
+00.    +05.    +11.    +01.    +60.
+00+00
9                           END OF CHUCK3 INPUT
```

Fig. 17. Examples of input files for the three transfer reactions. In the lower input file the specific values that have to be changed for each state are underlayed in grey. These are $l, J, \pi, n-1$ and E_x.

References

[1] D. Bucurescu, T. von Egidy, H.-F. Wirth, N. Marginean, U. Köster, G. Graw, A. Metz, R. Hertenberger, Y. Eisermann, Nucl. Phys. A 674 (2000) 11.
[2] D. Bucurescu, T. von Egidy, H.-F. Wirth, N. Marginean, W. Schauer, I. Tomandl, G. Graw, A. Metz, R. Hertenberger, Y. Eisermann, Nucl. Phys. A 672 (2000) 21.
[3] W. Schauer, C. Doll, T. von Egidy, R. Georgii, J. Ott, H.-F. Wirth, A. Gollwitzer, G. Graw, R. Hertenberger, B. Valnion, M. Grinberg, Ch. Stoyanov, Nucl. Phys. A 652 (1999) 339.
[4] V. Bondarenko, T. von Egidy, J. Honzátko, I. Tomandl, D. Bucurescu, M. Marginean, J. Ott, W. Schauer, H.-F. Wirth, C. Doll, Nucl. Phys. A 673 (2000) 85.
[5] R. Georgii, T. von Egidy, J. Klora, H. Lindner, U. Mayerhofer, J. Ott, W. Schauer, P. von Neumann-Cosel, A. Richter, C. Schlegel, R. Schulz, V.A. Khitrov, A. M Sukhovoj, A.V. Vojnov, J. Berzins, V. Bondarenko, P. Prokofjevs, L.J. Simonova, M. Grinberg, Ch. Stoyanov, Nucl. Phys. A 592 (1995) 307.
[6] C. Doll, H. Lehmann, H.G. Börner, T. von Egidy, Nucl. Phys. A 672 (2000) 3.
[7] J. Honzátko, I. Tomandl, V. Bondarenko, D. Bucurescu, T. von Egidy, J. Ott, W. Schauer, H.-F. Wirth, C. Doll, A. Gollwitzer, G. Graw, R. Hertenberger, B. Valnion, Nucl. Phys. A 645 (1999) 331.
[8] J. Ott, C. Doll, T. von Egidy, R. Georgii, M. Grinberg, W. Schauer, R. Schwengner, H.-F. Wirth, Nucl. Phys. A 625 (1997) 598.
[9] V. Bondarenko, T. von Egidy, H.-F. Wirth, A. Metz, Y. Eisermann, G. Graw, R. Hertenberger, L. Rubaček, Beschleunigerlaboratorium der Universität und Technischen Universität München, Jahresbericht, 1998, p. 18.
[10] J. Honzátko, et al., Nucl. Phys. A, in preparation.
[11] H.-F. Wirth, T. von Egidy, C. Doll, U. Köster, W. Schauer, I. Tomandl, J. Honzátko, V. Bondarenko, D. Bucurescu, G. Graw, Y. Eisermann, R. Hertenberger, A. Metz, in: S. Wender (Ed.), Capture Gamma-Ray Spectroscopy, Santa Fe 1999, in: AIP Conf. Proc., Vol. 529, American Institute of Physics, New York, 2000, p. 663.
[12] H.-F. Wirth, Ph.D. Thesis, Techn. Univ. München, 2001, http://tumb1.biblio.tu-muenchen.de/publ/diss/ph/2001/wirth.html.
[13] T. von Egidy, H.-F. Wirth, I. Tomandl, J. Honzátko, V. Bondarenko, D. Bucurescu, Y. Eisermann, G. Graw, R. Hertenberger, in: R. Casten (Ed.), Proc. Int. Symposion on Nuclear Stucture Physics, Göttingen 2001, World Scientific, New Jersey, 2001, p. 89.
[14] I. Tomandl, et al., Nucl. Phys. A, in press.
[15] P.G. Calway, H.D. Sharma, Nucl. Phys. A 156 (1970) 338.
[16] S. Ohya, T. Tamura, S. Kageyama, J. Phys. Soc. Jpn. 29 (1970) 1435.
[17] J. Honzátko, K. Konečný, F. Bečvář, E.A. Eissa, M. Králík, Z. Phys. A 299 (1981) 183.
[18] S. Galès, G.M. Crawley, D. Weber, B. Zwieglinski, Nucl. Phys. A 381 (1982) 173.
[19] W.H. Moore, G.K. Schlegel, S. O'Dell, A. Graue, J.R. Lien, Nucl. Phys. A 104 (1967) 327.
[20] R.K. Jolly, Phys. Rev. 136 (3B) (1964) 683.
[21] M.A.M. Shahabuddin, J.A. Kuehner, A.A. Pilt, Phys. Rev. C 23 (1) (1981) 64.
[22] Y. Tendow, Nucl. Data Sheets 77 (1996) 631.
[23] J. Honzátko, K. Konečný, I. Tomandl, J. Vacík, F. Bečvář, P. Cejnar, Nucl. Instrum. Methods A 376 (1996) 434.
[24] R.B. Firestone, in: V.S. Shirley (Ed.), Table of Isotopes, Wiley, New York, 1996.
[25] B. Krusche, K.P. Lieb, H. Daniel, T. von Egidy, G. Barreau, H.G. Börner, R. Brissot, C. Hofmeyr, R. Rascher, Nucl. Phys. A 386 (1982) 245.
[26] C.A. Stone, B.E. Zimmermann, C.E. Ford, P.F. Mantica Jr., W.B. Walters, in: R.W. Hoff (Ed.), Proc. Int. Conf. Capture Gamma-Ray Spectroscopy, Pacific Grove 1990, American Institute of Physics, New York, 1991, p. 431.
[27] L.V. Groshev, A.M. Demidov, N. Shadiev, J. Nucl. Phys. (USSR) 4 (2) (1966) 172.
[28] D.L. Bushnell, R.P. Chatuverdi, R.K. Smither, Phys. Rev. 179 (4) (1969) 1113.
[29] M.A. Lone, R.A. Leavitt, D.A. Harrison, At. Data Nucl. Data Tables 26 (1981) 511.
[30] M. Löffler, H.J. Scheerer, H. Vonach, Nucl. Instrum. Methods 111 (1973) 1.
[31] E. Zanotti, M. Bisenberger, R. Hertenberger, H. Kader, G. Graw, Nucl. Instrum. Methods A 310 (1991) 706.

[32] F. Rieß, Beschleunigerlaboratorium der Universität und Technischen Universität München, Jahresbericht, 1991, p. 168.
[33] R. Hertenberger, Y. Eisermann, H.-F. Wirth, G. Graw, Beschleunigerlaboratorium der Universität und Technischen Universität München, Jahresbericht, 2000, p. 70.
[34] H.-F. Wirth, H. Angerer, T. von Egidy, Y. Eisermann, G. Graw, R. Hertenberger, Beschleunigerlaboratorium der Universität und Technischen Universität München, Jahresbericht, 2000, p. 71.
[35] P.D. Kunz, Computer Code CHUCK3, University of Colorado, unpublished.
[36] C.M. Perey, F.G. Perey, At. Data Nucl. Data Tables 17 (1976) 1.
[37] W.W. Daehnick, J.D. Childs, Z. Vrcelj, Phys. Rev. C 21 (6) (1980) 2253.
[38] H. Dias, L. Losano, Phys. Rev. C 50 (3) (1994) 1377.
[39] K. Schreckenbach, Program LEVFIT, ILL, Grenoble, 1975.
[40] J.R. Swider, D.M. Mustillo, L.F. Conticchio, W.B. Walters, R.L. Paul, R.M. Lindstrom, in: J. Kern (Ed.), Proc. Int. Conf. Capture Gamma-Ray Spectroscopy, Fribourg 1993, World Scientific, Singapore, 1994, p. 335.
[41] S.F. Mughabghab, M. Davideenam, N.E. Holden, in: Neutron Resonance Parameters and Thermal Cross Sections, Vol. 1(A), Academic Press, New York, 1981.
[42] L. Seren, H.N. Friedlander, S.H. Turkel, Phys. Rev. 72 (1947) 888.
[43] S.K. Mangal, P.S. Gill, Nucl. Phys. 36 (1962) 542.
[44] V. Maxia, Nucl. Sci. Eng. 35 (1969) 88.
[45] G. Molnar, T. Belgya, R.B. Firestone, private communication, 2001.
[46] A. Arima, F. Iachello, Phys. Rev. Lett. 40 (1978) 385.
[47] F. Iachello, O. Scholten, Phys. Rev. Lett. 43 (1979) 679.
[48] O. Scholten, KVI internal report 252, 1982.
[49] O. Scholten, Computer code SPEC, unpublished.
[50] V.G. Solov'ev, Sov. J. Part. Nucl. 9 (1978) 343.
[51] S. Galès, Ch. Stoyanov, A.I. Vdovin, Phys. Rep. 166 (1988) 125.
[52] A.M. Lane, J.E. Lynn, Nucl. Phys. 17 (1960) 563.
[53] S.F. Mughabghab, Phys. Lett. B 81 (2) (1979) 93.
[54] I. Tomandl, V. Bondarenko, D. Bucurescu, J. Honzátko, T. von Egidy, H.-F. Wirth, G. Graw, R. Hertenberger, A. Metz, Y. Eisermann, in: S. Wender (Ed.), Capture Gamma-Ray Spectroscopy, Santa Fe 1999, AIP Conf. Proc., Vol. 529, American Institute of Physics, New York, 2000, p. 200.
[55] L. Koester, H. Rauch, E. Seymann, At. Data Nucl. Data Tables 49 (1991) 65.
[56] V. Bondarenko, J. Honzátko, I. Tomandl, D. Bucurescu, T. von Egidy, J. Ott, W. Schauer, H.-F. Wirth, C. Doll, Phys. Rev. C 60 (1999) 027302.
[57] V. Bondarenko, J. Honzátko, I. Tomandl, Z. Phys. A 354 (1996) 235.